Mon. Not. R. Astron. Soc. **390,** 1437–1452 (2008) doi:10.1111/j.1365-2966.2008.13703.x

The kinematic footprints of five stellar streams in Andromeda's halo★

S. C. Chapman,[1,2]†‡ R. Ibata,[3] M. Irwin,[1] A. Koch,[4] B. Letarte,[5] N. Martin,[6] M. Collins,[1] G. F. Lewis,[7] A. McConnachie,[2] J. Peñarrubia,[2] R. M. Rich,[4] D. Trethewey,[1] A. Ferguson,[8] A. Huxor[8] and N. Tanvir[9]

[1]*Institute of Astronomy, Madingley Road, Cambridge CB3 0HA*
[2]*Department of Physics and Astronomy, University of Victoria, Victoria, BC V8P 1A1, Canada*
[3]*Observatoire de Strasbourg, 11, rue de l'Université, F-67000 Strasbourg, France*
[4]*Department of Physics and Astronomy, University of California at Los Angles, LA California, USA*
[5]*California Institute of Technology, Pasadena, CA 91125, USA*
[6]*Max-Planck-Institut für Astronomie, Königstuhl 17, D-69117 Heidelberg, Germany*
[7]*Institute of Astronomy, School of Physics, A29, University of Sydney, NSW 2006, Australia*
[8]*Institute for Astronomy, University of Edinburgh, Royal Observatory, Blackford Hill, Edinburgh EH9 3HJ*
[9]*Department of Physics and Astronomy, University of Leicester, Leicester LE17RH*

Accepted 2008 July 8. Received 2008 June 16; in original form 2008 March 26

ABSTRACT

We present a spectroscopic analysis of five stellar streams ('A', 'B', 'Cr', 'Cp' and 'D') as well as the extended star cluster, EC4, which lies within Stream 'C', all discovered in the halo of M31 from our Canada–France–Hawaii Telescope/MegaCam survey. These spectroscopic results were initially serendipitous, making use of our existing observations from the DEep Imaging Multi-Object Spectrograph mounted on the Keck II telescope, and thereby emphasizing the ubiquity of tidal streams that account for ∼70 per cent of the M31 halo stars in the targeted fields. Subsequent spectroscopy was then procured in Stream 'C' and Stream 'D' to trace the velocity gradient along the streams. Nine metal-rich ([Fe/H] ~ -0.7) stars at $v_{\rm hel} = -349.5\,{\rm km\,s^{-1}}, \sigma_{v,{\rm corr}} \sim 5.1 \pm 2.5\,{\rm km\ s^{-1}}$ are proposed as a serendipitous detection of Stream 'Cr', with follow-up kinematic identification at a further point along the stream. Seven metal-poor ([Fe/H] ~ -1.3) stars confined to a narrow, 15 km s^{-1} velocity bin centred at $v_{\rm hel} = -285.6$, $\sigma_{v,{\rm corr}} = 4.3^{+1.7}_{-1.4}$ km s^{-1} represent a kinematic detection of Stream 'Cp', again with follow-up kinematic identification further along the stream. For the cluster EC4, candidate member stars with average [Fe/H] ~ -1.4, are found at $v_{\rm hel} = -282$ suggesting it could be related to Stream 'Cp'. No similarly obvious cold kinematic candidate is found for Stream 'D', although candidates are proposed in both of two spectroscopic pointings along the stream (both at $\sim -400\,{\rm km\ s^{-1}}$). Spectroscopy near the edge of Stream 'B' suggests a likely kinematic detection at $v_{\rm hel} \sim -330$, $\sigma_{v,{\rm corr}} \sim 6.9\,{\rm km\ s^{-1}}$, while a candidate kinematic detection of Stream 'A' is found (plausibly associated to M33 rather than M31) with $v_{\rm hel} \sim -170$, $\sigma_{v,{\rm corr}} = 12.5\,{\rm km\ s^{-1}}$. The low dispersion of the streams in kinematics, physical thickness and metallicity makes it hard to reconcile with a scenario whereby these stream structures as an ensemble are related to the giant southern stream. We conclude that the M31 stellar halo is largely made up of multiple kinematically cold streams.

Key words: stars: kinematics – galaxies: haloes – galaxies: individual: M31.

1 INTRODUCTION

Stellar streams represent the visible debris of small galaxies being cannibalized by large galaxies, memorials to the merging process by which the haloes of galaxies are built up. The best known examples of streams in the Milky Way (MW) have recently been mapped far more extensively by the Sloan Digital Sky Survey-Data Release 5 by Belokurov et al. (2006, 2007): the tidally stripped stars

★The data presented herein were obtained at the W. M. Keck Observatory, which is operated as a scientific partnership among the California Institute of Technology, the University of California and the National Aeronautics and Space Administration. The Observatory was made possible by the generous financial support of the W. M. Keck Foundation.

†E-mail: schapman@ast.cam.ac.uk
‡Canadian Space Agency, Space Science Fellow.

and globular clusters associated with the Sagittarius (Sgr) dwarf spheroidal and the low-latitude stream, along with a newly discovered 'Orphan Stream' so named for its lack of obvious progenitor. In M31, thanks to our ability to efficiently map vast regions of the halo, the number of discovered giant streams already outnumbers that of the MW (Ibata et al. 2007). However, of the eight stellar streams that have been identified in the halo of M31, only one has plausibly been identified to a dwarf satellite: the loop connecting to NGC 205 (McConnachie et al. 2005). This suggests that the other streams could represent an additional seven 'uncatalogued' satellites, although some of the streams might be produced by a common progenitor, as suggested by models of Fardal et al. (2007, 2008) for the M31 Giant Southern Stream, or in a similar fashion to the Sgr dwarf and its numerous wraps around the MW. It is important to characterize their orbits, metallicities and masses, to understand what their progenitors must have been.

The existence of stellar streams tells us that a progenitor galaxy has undergone significant mass-loss. This is due to a combination of its orbit and phase of evolution – the amount of dark matter mass the galaxy has lost (Peñarrubia, McConnachie & Navarro 2008a; Peñarrubia, Navarro & McConnachie 2008b). Satellites on circular orbits are harder to disrupt, but if they are massive enough [i.e. of the order of the Large Magellanic Cloud (LMC)], dynamical friction will bring them close to the host galaxy centre, where the interactions with the disc will lead to their tidal disruption – e.g. Peñarrubia et al. 2007. In addition, to form a stream one has to remove most of the dark matter halo (∼90–99 per cent). The most important parameter that controls the mass-loss rate of a dSph is the pericentre distance (the orbital eccentricity is of second order). On the other hand, dwarfs with highly elliptical orbits spend a lot of time near apocentre where they are unlikely to be disrupted by the host. It is therefore not immediately obvious that streams represent preferred types of orbits on average. However, a number of theoretical studies have shown that significant information about the orbital properties of the progenitor galaxy can be derived from the streams (e.g. Ghigna et al. 1998; Helmi et al. 1999).

Streams can be much more informative to study than dwarfs because their orbits can be directly traced and constrained. Fellhauer et al. (2006) were able to accurately constrain the shape of the Galactic potential through the bifurcation of Sgr streams in Belokurov et al. (2006). Understanding the range of orbits of satellites to large galaxies will help us to understand how the haloes of these galaxies formed. This is especially interesting in light of M31's huge stellar halo reflecting the dark matter dominated halo out to $\gtrsim$150 kpc (e.g. Irwin et al. 2005; Gilbert et al. 2006; Ibata et al. 2007). However, streams can also be much harder to analyse observationally: the distances are problematic, there is a much lower spatial density and they have a larger extent so that observational sampling is not trivial. There is also the difficulty to infer the membership of different stream pieces, especially if we expect different chemical signatures due to metallicity gradients in the progenitor system (e.g. Ibata et al. 2007).

Streamy/blobby structures are individually interesting and constraining for the halo formation. They can represent the only traceable product of long disintegrated progenitors, yet retain a coherent body for statistical analysis. Streams can provide important clues on the structure of the progenitors (e.g. metallicity gradients, mass-to-light ratio – M/L) as well as on the shape of the host dark matter halo (e.g. prolate versus oblate) (Martinez-Delgado et al. 2008). Future study of these structures will be able to put them in a much better 'near-field cosmology' context, eventually understanding their ages and chemical histories. However, it is important to uncover and study them now, even in limited capacities necessitated by the small numbers of spectroscopically identifiable stars and Hertzsprung–Russell diagram depths, so we can build our models on the most complete context.

We have initiated a spectroscopic survey of the new streams found in M31's halo using the DEep Imaging Multi-Object Spectrograph (DEIMOS) on Keck II to derive radial velocities and metallicities of red giant branch (RGB) stars. In this contribution, we discuss spectroscopic pointings in each of streams 'C' and 'D' which we obtained by serendipity, since the spectroscopy was taken prior to knowledge of the photometrically discovered streams, as well as follow-up spectroscopic pointings in both of these streams. We also analyse spectroscopic data from Koch et al. (2008) lying within the Ibata et al. (2007) streams 'A' and 'B'.

2 OBSERVATIONS AND ANALYSIS

The spectroscopic fields along the M31 minor axis discussed in this paper are highlighted in Fig. 1, two lying at ∼35 kpc, three lying at ∼60 kpc, one at ∼80 kpc and one at ∼120 kpc projected from the centre of M31. The fields cover the four stellar streams presented in the Ibata et al. (2007) M31 extended halo analysis, called Stream 'D', 'C', 'B' and 'A', respectively. In these M31 halo images, it can be seen that Stream 'C' has significantly different morphology as a function of metallicity, a more metal-rich component dominating the structure, with a more irregular shaped metal-poor component to the east. While it was not proposed initially, our evidence in this work suggests the two structures may be distinct systems, and we refer to these as two separate streams, Stream 'Cr' for the metal-rich component and Stream 'Cp' for the metal-poor component (this issue is explored in detail in Section 3.3 and Figs 10 and 11).

Multi-object spectroscopic observations with the Keck II telescope and the DEIMOS – DEIMOS (Davis et al. 2003) were obtained in photometric conditions with ∼0.8 arcsec seeing in 2004 and 2005 September. Target stars were chosen by colour/magnitude selection as described in Ibata et al. (2005), first selecting likely RGB stars in M31 over all metallicities and filling space with any other stellar objects in the field. Two spectroscopic masks (F25 and F26 from the table in Chapman et al. 2006) targeted the field of an extended cluster EC4 (Mackey et al. 2006), which were found after the fact to be spanning Stream 'Cr' and Stream 'Cp'. A combined total of 212 independent stars in both masks were observed in standard DEIMOS slit-mask mode (Davis et al. 2003) using the high-resolution 1200 line/mm grating and 1 arcsec width slitlets. 10 of these target stars were specifically selected from *Hubble Space Telescope* (*HST*) photometry of EC4 to lie within the cluster. Our instrumental setting covered the observed wavelength range from ∼0.70 to 0.98 μm. Exposure time was 60 min, split into 20-min integrations. The DEIMOS-DEEP2 pipeline (Faber et al. 2003) designed to reduce data of this type accomplishes tasks of debasing, flat-fielding, extracting, wavelength calibrating and sky subtracting the spectra. The same settings were used to target a halo field which was found after the fact to lie in Stream 'D'. 89 stars were observed in this mask (F7).

The Ibata et al. (2007) imaging discovery of the new streams, coupled with obvious kinematic detection of the Stream 'Cr' and Stream 'Cp' in our existing spectroscopic observations (described in subsequent sections) prompted the follow-up study of these structures. On 2007 October 8, additional DEIMOS masks were obtained further along the Stream 'C' and Stream 'D', as identified in Fig. 1 and Table 1. These observations were obtained under ∼1 arcsec

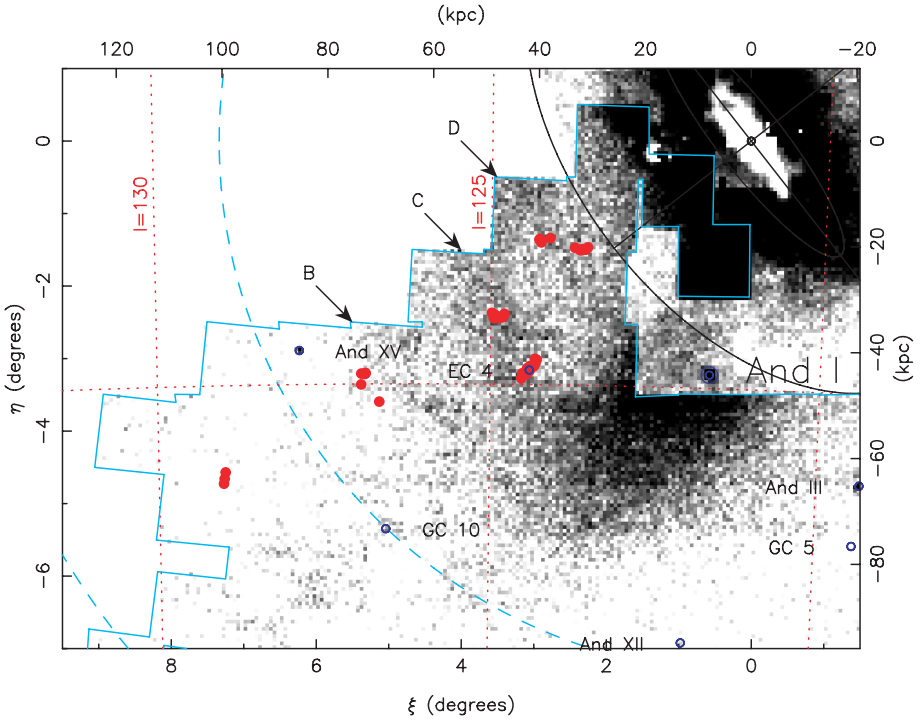

Figure 1. The locations of the spectroscopic measurements (red circles) are overlaid on the imaging data from the INT and CFHT telescopes presented in Ibata et al. (2007). Streams 'B', 'C' and 'D' intersect the minor axis of M31 approximately perpendicularly at ∼80, ∼ 60 and ∼35 kpc, respectively. The irregular turquoise line demarks the CFHT survey region. The scale of the diagram is shown by the circle segment (dashed line – marking a projected radius of 100 kpc), as well as by the ellipse segment (continuous line – showing a 50 kpc ellipse of axis ratio 0.6). Two of the newly discovered dwarf spheroidals from our survey are visible in the same region, And XII (Martin et al. 2006; Chapman et al. 2007) and And XV (Ibata et al. 2007; Letarte et al. 2008).

Table 1. Properties of DEIMOS fields in the M31 stellar streams 'A','B','C' and 'D'.

Field	α (J2000), δ (J2000)	$v_{\rm r,stream}$	$\sigma_{\rm stream}{}^a$ (km s^{-1})	$\langle$[Fe/H]$\rangle^b$ (km s^{-1})	$w_{\rm stream}{}^c$ (kpc)	$R_{\rm peri}{}^d$ (kpc)	$M_{\rm stream}{}^e$ $\times 10^7$ M$_\odot$	$L_{\rm stream}{}^f$ $\times 10^6$ L$_\odot$
Stream A (M8)	01:14:01.37 +32:31:00.9	−172.2	12.5	-1.3 ± 0.3 (-1.3)	7.5	24	10/7	2.3
Stream B (M6)	01:32:14.64 +33:12:25.4	−330.1	6.9	-0.8 ± 0.2 (-0.6)	5.0	16	7/2	10.0
Stream Cr (F25/F26)	00:58:22.02 +38:04:05.9	−349.5	5.1 ± 2.5	-0.7 ± 0.2 (-0.6)	6.8	12	30/1	12.6
Stream Cp (F25/F26)	00:58:22.02 +38:04:05.9	−287.3	$4.3^{+1.7}_{-1.4}$	-1.3 ± 0.2 (-1.1)	8.5	11	70/1	1.4
Stream Cr pos2 (F36)	01:00:38.00 +38:45:37.0	−350	n/a	-0.7 ± 0.2 (-0.6)	n/a			
Stream Cp pos2 (F36)	01:00:38.00 +38:45:37.0	−246	n/a	-1.2 ± 0.2 (-1.1)	n/a			
Stream D (F7)	00:54:55.02 +39:43:55.3	−390.5	4.2	-1.1 ± 0.3 (-1.2)	8.2	6	213/1	9.5
Stream D pos2 (F37)	00:57:34.00 +39:49:12.0	−390.5	4.2	-1.1 ± 0.3 (-1.2)	n/a			
EC4 (F25/F26)	00:58:15.50 +38:03:01.1	−282.4	∼10	-1.4 ± 0.1	n/a			

[a] Velocity dispersions, estimated through a maximum-likelihood analysis taking into account the measurement errors in the velocities (or in the case of Stream 'A', Stream 'B', Stream 'D', a subtraction in quadrature of the measurement error).
[b] For certain streams (notably Stream 'A' and Stream 'D'), it is arguable that the [Fe/H]$_{\rm phot}$ measurements are estimated from sets of stars which may not actually be a kinematic detection of 'the stream'. For this reason, we also quote the statistical [Fe/H]$_{\rm phot}$ estimate from Ibata et al. (2007) in all cases in brackets. In particular, the Stream 'D' values are quoted for the combination of six stars in the two separated pointings along the stream, and therefore the numbers in the table are simply duplicated.
[c] Stream widths derived from Gaussian fits (quoted FWHM) to the integrated profile in the region defined in Ibata et al. (2007) (their fig. 31). At the distance of M31 (785 kpc – McConnachie et al. 2005) $1^\circ = 13$ kpc.
[d] $R_{\rm peri}$ estimated as 1/5 $D_{\rm stream}$ as discussed in the text.
[e] Mass of stream width estimated from structural parameters (first entry) and from σ_v (second entry).
[f] $L_{\rm stream}$ from Ibata et al. (2007), except for Stream 'Cp', Stream 'Cr', which are discussed in the text.

seeing, and cloudy conditions. For the field F36, we obtained 3 × 20 min integrations on a mask with 113 targeted stars, while field F37 was observed for 4 × 20 min integrations with 138 targeted stars. These observations used the lower resolution 600 l/mm grating to achieve a higher signal-to-noise ratio (S/N) in the continuum for the fainter stars, and resulting in a resolution of ∼3 Å estimated from the width of sky lines.

The radial velocities of the stars in all these fields were then measured with respect to spectra of standard stars observed during the observing runs. By fitting the peak of the cross-correlation

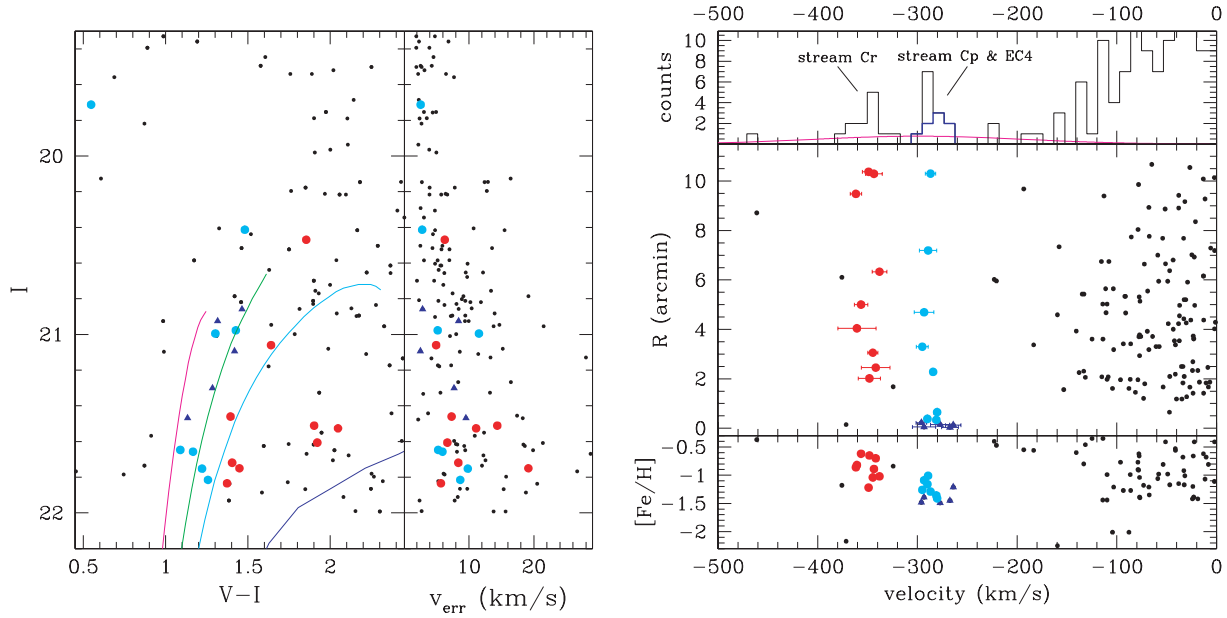

Figure 2. Left-hand panel: CFHT-MegaCam CMD and radial velocity uncertainties of the observed stars in the Stream 'Cr'/Stream 'Cp' fields. Stars likely belonging to Stream 'Cr' (red), Stream 'Cp' (cyan) and EC4 (blue) are highlighted. The bright and very blue star belonging to Stream 'Cp' is unusual for M31 and its properties are described in the text. The fiducial RGBs correspond to, from left- to right-hand side, NGC 6397, NGC 1851, 47 Tuc, NGC 6553 which have metallicity of [Fe/H] = −1.91, −1.29, −0.71 and −0.2, respectively. These fiducials have been shifted to the average distance modulus of EC4, 24.47 (785 kpc – Mackey et al. 2006). Right-hand panel: the velocities of observed stars in the F25/F26 fields are shown as a histogram, with EC4 member stars highlighted as a heavy histogram. The stellar halo velocity dispersion (σ_v = 125 km s^{-1}) from Chapman et al. (2006) is shown normalized to the expected nine halo stars at this position from Ibata et al. (2007). To differentiate EC4 stars from the field, we additionally plot the velocities against their radius from the EC4 centre (Table 1), referencing the symbols to the CMD plot. Photometrically derived [Fe/H] is shown as a function of radial velocity, again referenced in symbol type to the CMD plot.

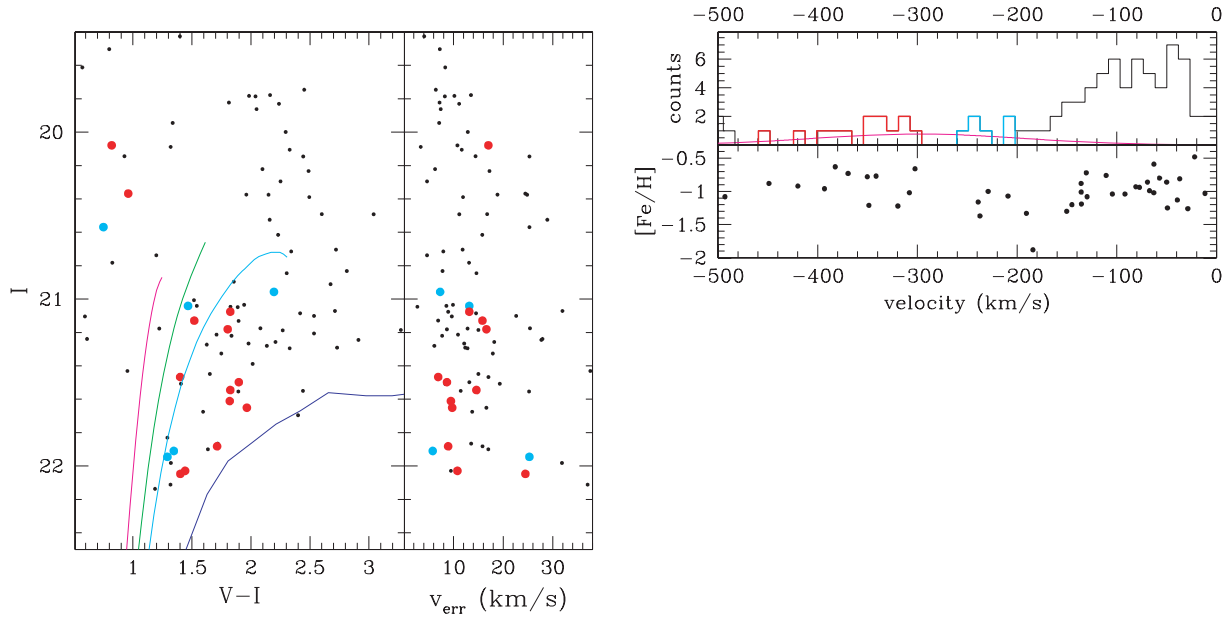

Figure 3. The same as for Fig. 2 for a field further along the Stream 'C' structure (F36). While no similarly obvious kinematic peaks are detected as in Fig. 2, we highlight stars potentially belonging to Stream 'Cr' (red) and Stream 'Cp' (cyan).

function, an estimate of the radial velocity accuracy was obtained for each radial velocity measurement. The accuracy of these data, as estimated from the Calcium Triplet (CaT) cross-correlation, varies with magnitude, having uncertainties of $<$10 km s^{-1} for most of the stars. The colour–magnitude diagrams (CMDs), velocity errors, velocity histograms and metallicities for these fields are shown in Figs 2 and 3 for Stream 'C', and Figs 4 and 5 for Stream 'D'. Spectroscopic metallicities quoted in these tables are calculated from the equivalent widths of the Ca II triplet lines, as described in Ibata et al. (2005).

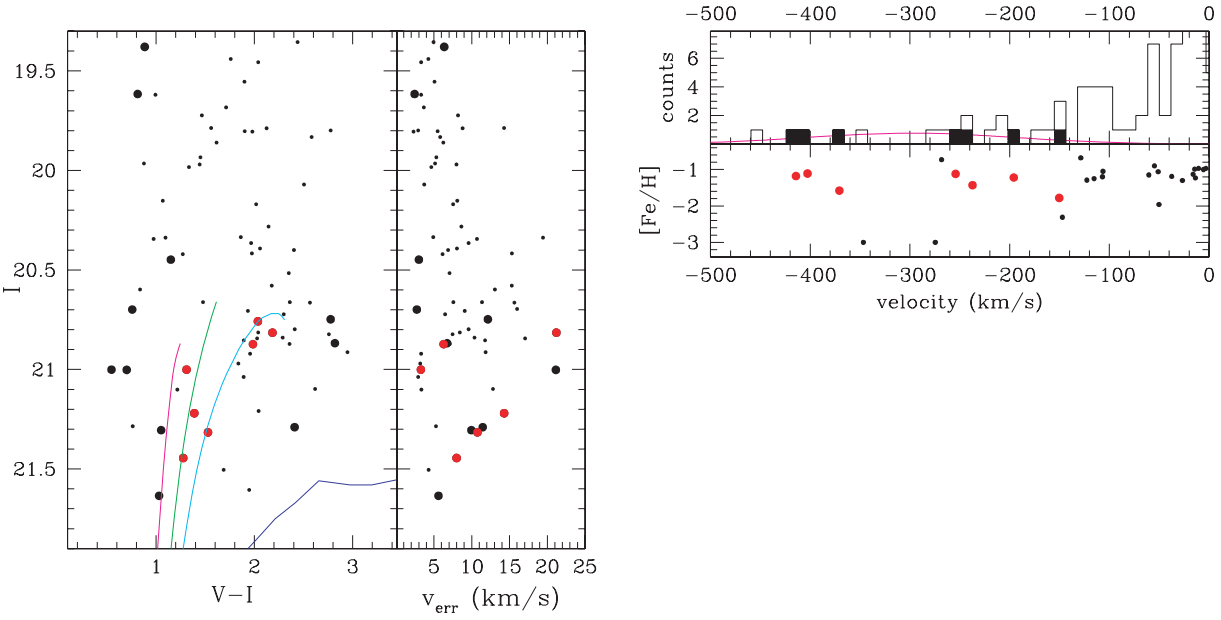

Figure 4. Left-hand panel: CFHT-MegaCam CMD and radial velocity uncertainties of the observed stars in the Stream 'D' field (F7). The fiducial RGBs are as in Fig. 2, shifted to the same average distance modulus of M31, 24.47, 785 kpc (McConnachie et al. 2005). Large symbols represent stars unlikely to be contaminated by foreground MW ($v_{\rm hel} < -150$ km s^{-1}). Symbols are further highlighted which have photometric metallicities consistent with the [Fe/H] distribution of Stream 'D' in Ibata et al. (2007): $-1.7 <$ [Fe/H] < -0.7. Right-hand panel: the velocities of observed stars in the Stream 'D' field are shown as a histogram, with possible Stream 'D' stars from the left-hand panel highlighted as a filled histogram. Photometrically derived [Fe/H] is shown as a function of radial velocity, and referenced in symbol type to the CMD plot.

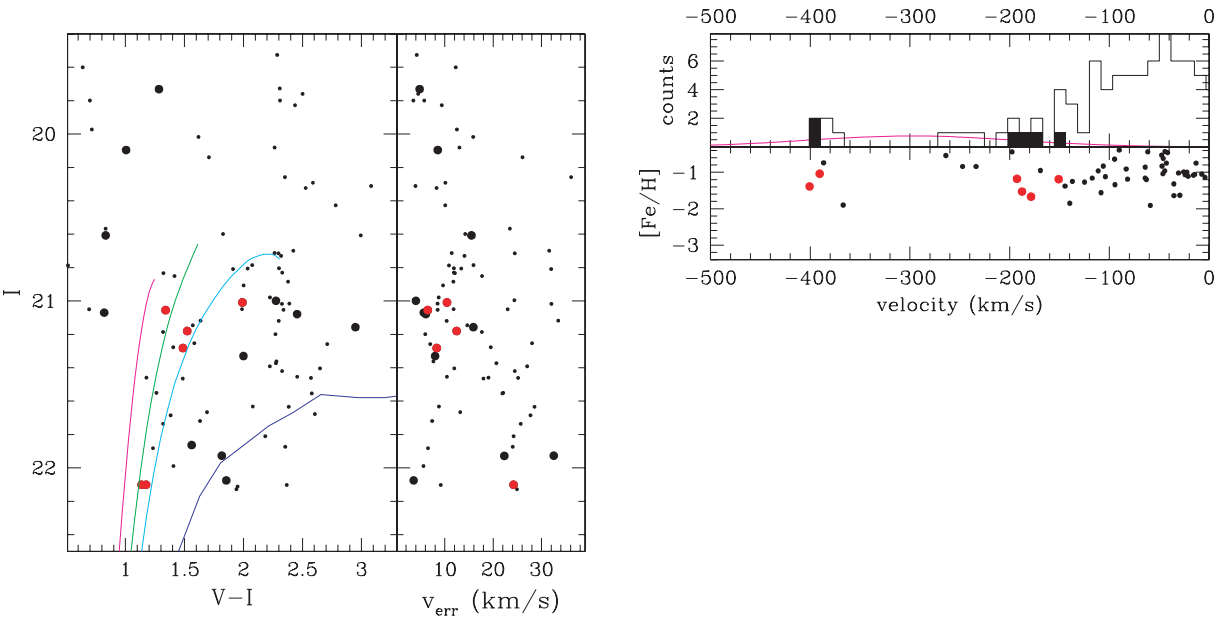

Figure 5. The same as for Fig. 4 for a field further along the Stream 'D' structure (F37). Symbols are again highlighted which have photometric metallicities consistent with the [Fe/H] distribution of Stream 'D' in Ibata et al. (2007): $-1.7 <$ [Fe/H] < -0.7.

Finally, the two furthest streams along the minor axis from Ibata et al. (2007), Stream 'A' and Stream 'B' lying at 120 and 80 kpc, respectively, have serendipitous DEIMOS spectroscopic pointings lying in their edge regions from Gilbert et al. (2006) and Koch et al. (2008) (fields M8 and M6, respectively). Reduction and analysis of these two fields are detailed in Koch et al. (2008). Figs 6 and 7 show the CMDs and velocity/metallicity distributions for Stream 'B' and Stream 'A', respectively.

We address Galactic contamination to our spectroscopically identified stars in a manner identical to Koch et al. (2008), using a combination of $v - I$ radial velocity and the equivalent width (EW) of Na $I_{\lambda 8183,8195}$ which is sensitive to surface gravity, and is accordingly very weak in M31 RGB star spectra, but can be strong in Galactic dwarfs (Schiavon et al. 1997). At velocities $v_{\rm hel} < -150$ km s^{-1}, very few RGB candidates show any significant Na $I_{\lambda 8183,8195}$ absorption lines, whereas stars with -150 to 0 km s^{-1} velocity show strong

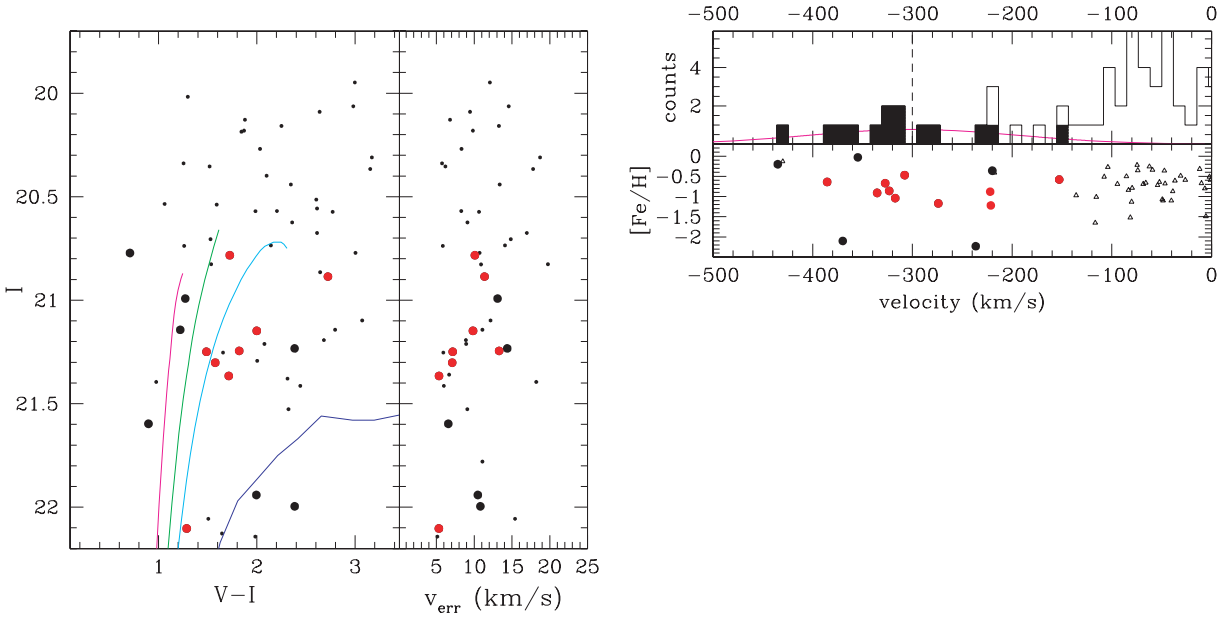

Figure 6. The same as for Fig. 5 for stars in the Stream 'B' field, named 'M6' from Gilbert et al. (2006) and Koch et al. (2008). Symbols are again highlighted which have photometric metallicities consistent with the [Fe/H] distribution of Stream 'B' in Ibata et al. (2007).

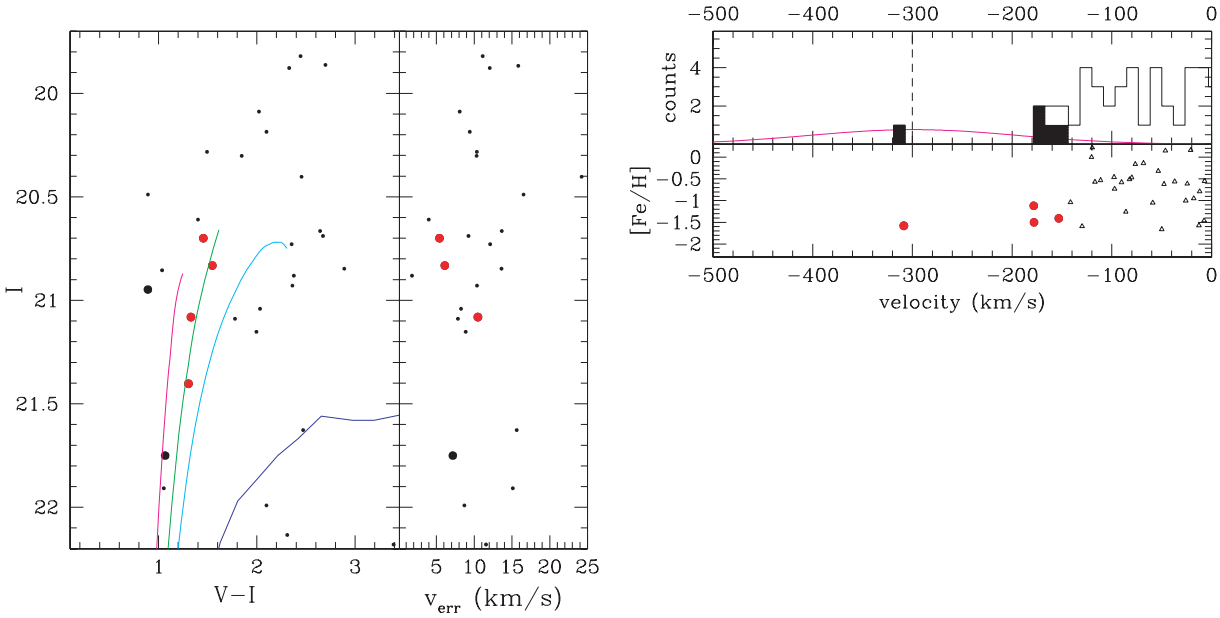

Figure 7. The same as for Fig. 5 for stars in the Stream 'A' field, named 'M6' from Gilbert et al. (2006) and Koch et al. (2008). Symbols are again highlighted which have photometric metallicities consistent with the [Fe/H] distribution of Stream 'A' in Ibata et al. (2007).

Na I absorption on average, consistent with the findings of Chapman et al. (2006), Guhathakurta et al. (2006), Gilbert et al. (2006) and Koch et al. (2008). For this study, we impose the additional constraint of removing all stars from the halo sample with $v_{\rm hel} > -150$ km s^{-1}, and we remove any stars from our sample which have a summed EW(Na I$_{\lambda 8183,8195}$) > 0.8 in the velocity range $v_{\rm hel} < -150$ km s^{-1}.

The properties of all candidate M31 halo (and stream) stars in these fields are listed in Tables 2–7, including coordinates, velocities, spectroscopic and photometric metallicities, and v, I photometry.

2.1 Observations of the cluster, EC4

The two minor-axis stellar halo fields, F25/F26, lying serendipitously in Stream 'C' were observed with the additional goal of constraining the kinematics of an 'extended star cluster', EC4. These extended, luminous objects in the outskirts of M31 represent a population with ∼15–60 kpc projected radii, large half-light radii for GCs with luminosities near the peak of the GC luminosity function (Huxor et al. 2005, 2008). As such, they are dissimilar to any other known clusters in the MW or M31, and begin to fill in the gap in parameter space between classical globular clusters and dwarf

Table 2. Properties of candidate M31 halo stars in stream D_1 region (field F7).

α (J2000)	δ (J2000)	v_r (km s^{-1})	v_{err} (km s^{-1})	[Fe/H]$_{phot}$	[Fe/H]$_{spec}$	v mag	I mag
00:54:18.02	+39:43:32.4	−449.7	6.4	–	−3.12	20.26	19.38
00:54:26.77	+39:45:58.2	−150.3	3.2	−1.78	−2.027	22.31	21
00:54:31.71	+39:44:54.1	−346.7	9.96	−3	−1.662	22.36	21.3
00:54:35.93	+39:43:59.2	−402.7	11.05	−1.11	−3.295	22.84	21.32
00:54:39.48	+39:45:05.4	−169.4	34.95	–	−2.181	21.7	21
00:54:40.93	+39:43:08.8	−268.4	11.45	−0.73	−2.843	23.7	21.29
00:54:47.03	+39:44:25.9	−370.8	8.01	−1.58	−3.454	22.72	21.44
00:54:50.30	+39:43:36.5	−237.3	14.53	−1.43	−2.144	22.61	21.22
00:54:53.48	+39:43:11.3	−274.6	5.46	−3	−2.637	22.66	21.64
00:54:57.75	+39:43:32.5	−195.9	49.42	−1.22	−3.394	22.79	20.76
00:55:00.87	+39:43:37.5	−254.2	25.61	−1.12	−3.135	23	20.82
00:55:10.40	+39:46:58.7	−162.1	2.73	–	−2.025	21.46	20.7
00:55:12.94	+39:43:50.3	−151.5	2.44	–	−2.427	20.43	19.62
00:55:13.27	+39:43:19.4	−211.5	7.26	–	−2.894	23.69	20.87
00:55:14.67	+39:44:52.5	−217.8	38.62	–	−3.182	21.55	21
00:55:22.81	+39:45:25.5	−414.3	8.37	−1.18	−1.537	22.86	20.87
00:55:27.67	+39:43:25.5	−244.2	3.11	–	−2.73	21.42	19.16
00:55:34.22	+39:42:51.8	−212.3	12.14	–	−2.776	23.52	20.75

Table 3. Properties of candidate M31 halo stars in stream D_2 region (field F37).

α (J2000)	δ (J2000)	v_r (km s^{-1})	v_{err} (km s^{-1})	[Fe/H]$_{phot}$	[Fe/H]$_{spec}$	v mag	I mag
00:56:58.88	+39:50:08.3	−203.6	9.94	–	−1.384	19.75	18.35
00:57:02.80	+39:47:56.0	−150.9	12.45	−1.19	0.4212	22.7	21.18
00:57:06.19	+39:49:49.9	−178.6	6.47	−1.67	0.3611	22.39	21.05
00:57:09.96	+39:52:32.5	−366.9	15.91	−1.9	−1.331	24.11	21.16
00:57:35.45	+39:49:42.4	−187.6	24.21	−1.53	2.214	23.24	22.1
00:57:37.07	+39:47:50.2	−153.3	4.8	–	−0.9179	21.02	19.73
00:57:40.78	+39:50:55.2	−264	32.52	−0.54	−0.5198	23.74	21.93
00:57:41.37	+39:48:33.1	−197.6	3.56	−0.44	1.305	23.93	22.07
00:57:43.61	+39:51:13.5	−192.6	8.33	−1.18	−0.3217	22.77	21.28
00:57:47.86	+39:50:35.0	−400.6	43.33	−1.39	−0.605	23.28	22.1
00:57:48.24	+39:48:36.6	−390.5	10.44	−1.04	−0.3352	23	21.01
00:57:50.48	+39:49:09.6	−169.2	4.03	−0.95	−1.017	23.27	21
00:57:55.32	+39:51:25.7	−386.6	6.08	−0.74	−0.2843	23.53	21.08
00:57:56.65	+39:50:48.5	−385.6	8.55	–	−0.9452	21.1	20.1
00:57:57.41	+39:51:43.2	−233.7	55.17	−0.84	−1.161	23.42	21.86
00:58:00.09	+39:48:33.5	−247.3	7.99	−0.84	−0.3931	23.33	21.33
00:58:06.18	+39:51:15.1	−258.6	15.52	–	−1.195	21.44	20.61

spheroidal galaxies. The 'faint fuzzies' discovered in NGC 1023 (Larsen & Brodie 2000; Brodie & Larsen 2002), and the similarly diffuse objects in the ACS Virgo Cluster survey (Peng et al. 2006), may represent a similar class of cluster. EC4 was discovered within the Canada–France–Hawaii Telescope-MegaCam (CFHT-MegaCam) survey (Huxor et al. 2008) at a projected radius of 60 kpc (coordinates in Table 1).

10 stars were selected to lie within EC4 by their CMD colours. Of these 10, one was subsequently identified as a galaxy in the HST/ACS image (Mackey et al. 2006), while another lies well off the cluster RGB, likely due to contamination in the ground-based CFHT-MegaCam imaging affecting the colour measurements. The remaining eight stars are candidate EC4 members, lying within five core radii of the cluster centre and falling along the top of the narrow RGB from the *HST* imagery (see Collins et al., in preparation).

In Fig. 2, the MegaCam photometry is shown for EC4 stars for consistency with the stream data. However, comparison with the very narrow RGB from *HST* photometry in Mackey et al. (2006) shows that crowding affects the ground-based accuracy, since the scatter on the MegaCam CMD is much larger than the difference in photometric errors (*HST* to MegaCam) would warrant. In Collins et al. (in preparation), the *HST* photometry for the EC4 stars is shown transformed to the MegaCam filter system. In analysing the DEIMOS spectroscopy, one targeted star lay exactly on the EC4 CMD, but had a discrepant velocity from the others. A closer examination of the spectrum revealed good detections of the first and second CaT lines with a velocity of -277.3 km s^{-1}, whereas the automated software pipeline derived a cross-correlation fit to larger skyline residuals. We include this eighth star in the catalogue as a viable member of EC4.

2.2 Velocity accuracy: repeat measurements of stars in fields F25 and F26

While CaT fitting errors suggest relatively small velocity errors, an independent check can be made on the 56 radial velocities of stars lying in spectroscopic masks of both fields F25 and F26. Velocity differences are shown in Fig. 8 highlighting those corresponding to

Table 4. Properties of candidate M31 halo stars in stream C_1 region (field F25/F26).

α (J2000)	δ (J2000)	v_r (km s^{-1})	v_{err} (km s^{-1})	[Fe/H] $_{phot}$	[Fe/H] $_{spec}$	v mag	I mag	D_{EC4}[a]
00:57:46.69	+38:11:43.0	−349	6.3	−1.22	−1.28	22.49	20.47	10.38
00:57:48.22	+38:11:48.6	−343.6	8.38	−0.89	−4.83	23.29	21.72	10.3
00:57:51.02	+38:11:25.4	−193.3	5.69	−0.55	−1.75	23.74	21.83	9.68
00:57:52.27	+38:08:34.6	−289.3	8.68	−1.01	−1.76	23.24	21.82	7.19
00:57:54.36	+38:12:26.8	−286.9	5.21	−1.29	−0.63	22.57	20.98	10.3
00:57:56.30	+38:06:18.1	−356.5	6.7	−0.62	2.75	23.7	21.61	5.00
00:58:05.23	+38:08:41.4	−223	2.22	−0.4	−1.8	24.27	21.48	6.02
00:58:12.75	+38:05:24.6	−341.8	14.37	−0.7	−0.97	23.58	21.51	2.45
00:58:13.99	+38:06:18.1	−295.1	5.96	−1.26	−1.09	22.99	21.66	3.30
00:58:14.37	+38:03:00.4	−296	5.29	−1.48	−1.84	22.91	21.65	0.22
00:58:14.74	+38:03:00.8	−277.3	9.56	−1.49	−5.62	22.77	21.47	0.15
00:58:15.24	+38:03:01.3	−293.4	11.55	−1.39	−1.89	21.7	20.99	0.05
00:58:15.32	+38:03:09.7	−371.5	10.9	−2.17	0.63	22.65	21.57	0.15
00:58:15.47	+38:02:58.9	−267.4	8.42	−1.45	−0.53	22.41	20.92	0.04
00:58:15.94	+38:04:34.9	−153.3	40.28	−2.45	3.38	22.78	21.73	1.57
00:58:15.99	+38:02:56.1	−264	7.74	−1.21	−0.69	22.75	21.3	0.13
00:58:16.00	+38:02:22.5	−280.3	2.83	−1.41	−1.38	22.06	20.41	0.65
00:58:17.12	+38:02:54.1	−281	2.9	−1.36	−0.65	22.49	20.86	0.34
00:58:17.16	+38:02:49.6	−290	2.57	−1.16	−1.12	22.68	21.09	0.38
00:58:18.62	+38:00:16.7	−530.7	9.81	–	0.73	24.18	20.6	2.81
00:58:19.68	+38:06:42.4	−577.2	11.45	−0.77	−2.2	23.5	21.11	3.78
00:58:20.25	+37:59:46.6	−183.4	19.86	−0.56	−0.96	23.84	21.65	3.37
00:58:21.87	+38:00:13.9	−344.7	4.98	−1.04	−0.69	22.87	21.06	3.06
00:58:22.02	+38:04:05.9	−324.3	20.49	−0.84	2.1	23.39	21.84	1.68
00:58:23.15	+37:58:40.9	−159.6	8.61	−2.25	−1.27	22.26	21.1	4.59
00:58:24.32	+38:04:29.9	−284.3	2.6	–	−3.06	20.43	19.71	2.28
00:58:25.71	+38:03:12.2	−348.1	11.12	−0.65	−0.1	23.74	21.53	2.02
00:58:29.49	+38:00:03.6	−360.7	19.15	−0.82	−0.2	23.37	21.75	4.04
00:58:32.37	+37:59:42.3	−293.3	9.84	−1.09	−0.98	23.14	21.75	4.69
00:58:34.09	+37:56:39.3	−157.9	2.34	–	−2.22	21.33	20.81	7.34
00:58:41.07	+37:55:54.7	−461.1	8.3	−0.37	−1.34	24.16	21.91	8.71
00:58:42.74	+38:00:24.9	−220.8	3.74	−0.47	−1.52	23.98	21.44	5.96
00:58:43.46	+38:00:22.4	−375.8	8.44	−1.18	−0.7	22.84	20.86	6.11
00:58:44.18	+38:00:08.9	−338	7.35	−1.02	−1.35	23.02	21.46	6.33
00:58:47.15	+37:55:52.5	−361.7	5.72	−0.86	−1.55	23.38	21.83	9.48

[a]Distance from the centre of EC4 in arcmin. At the distance of EC4, 13 kpc = 1°.

Stream 'C' (three stars), Stream 'D' (two stars), EC4 (three stars), background halo (two stars) and MW foreground (46 stars). A systematic shift from night 1 to night 2 of 3 km s^{-1} was found over all velocities, and this has been removed as a constant. Agreement between observing nights for these stars is then generally found within the 1σ errors of the radial velocity measurements, suggesting that no significant skew from mask misalignments or systematic errors is present from instrumental setup night to night. The dispersion in velocity differences is $\sim$6 km s^{-1} for both the M31 sample and the MW sample taken separately, which is comparable to the typical velocity measurement error of an individual star. For these 56 stars, we have taken as the radial velocity the error-weighted average of the measurement from the two nights.

3 RESULTS

3.1 Global kinematics and metallicities of the fields

Figs 2–7 (left-hand panels) show the CFHT-MegaCam (CMD) and radial velocity uncertainties of the observed stars in the Stream 'C', 'D', 'B' and 'A' fields, while the right-hand panels show velocity histograms and photometrically derived metallicities, [Fe/H] = $\log(Z/Z_{\odot})$, are computed for the stars by interpolating between 10-Gyr old Padova isochrones (Girardi et al. 2004). The fixed age adopted for metallicity comparison to the fiducials will, of course, introduce a systematic uncertainty if they are not all old. Given that younger populations have been detected in the halo of M31, and that these streams could represent progenitors with a range of properties, we provide an estimate of the age variations on the [Fe/H] determinations. If 5-Gyr old isochrones are used, the apparent metallicity would shift by 0.2 dex more metal-rich. The average distance modulus of M31 is adopted, 24.47, 785 kpc (McConnachie et al. 2005). Stars which are unlikely to be contaminated by foreground MW ($v_{hel} < -150$ km s^{-1}) are highlighted. While spectroscopic metallicities are quoted in the tables, we do not use them for analysis here as the errors on individual star measurements are so large as to broaden the typical [Fe/H] distribution by a factor of 3 for a stream kinematic structure. While the photometric [Fe/H] determinations are highly model dependent, the distributions for a given structure are likely far more reliable than those measured from the relatively low S/N spectroscopy.

3.2 Stream 'Cr'

Stream 'C' is the dominant stellar component at the position of our spectroscopic masks F25/F26, exceeding the halo stars as well as

Table 5. Properties of candidate M31 halo stars in stream C_2 region (field F36).

α (J2000)	δ (J2000)	v_r (km s^{-1})	v_{err} (km s^{-1})	[Fe/H] $_{phot}$	[Fe/H] $_{spec}$	v mag	I mag
01:00:01.15	+38:44:42.5	−150.3	71.98	−1.3	−2.132	23.32	22.14
01:00:02.17	+38:47:18.9	−212.4	5.96	–	−2.05	19.74	18.54
01:00:02.65	+38:46:11.4	−164.5	21.39	–	−2.101	21.39	19.12
01:00:03.35	+38:46:38.3	−308	8.92	−1.02	−1.052	22.9	21.08
01:00:05.16	+38:44:44.3	−237.3	13.17	−1.37	−2.313	22.51	21.04
01:00:05.98	+38:45:08.8	−184.2	12.84	−1.88	−2.384	22.4	21.18
01:00:07.06	+38:45:41.5	−209.1	5.81	−1.07	−1.145	23.26	21.91
01:00:10.97	+38:48:13.5	−348.6	6.91	−1.21	−0.940	22.65	21.13
01:00:12.06	+38:47:41.6	−190.8	53.77	−1.33	−1.991	22.52	21.01
01:00:15.76	+38:46:00.4	−448.9	9.47	−0.88	−1.234	23.47	22.03
01:00:17.03	+38:45:40.0	−350.3	14.61	−0.78	−1.159	23.37	21.54
01:00:20.95	+38:45:43.5	−369.6	9.73	−0.73	−1.252	23.43	21.61
01:00:23.72	+38:45:44.2	−630.9	9.66	–	−2.244	21.7	21.1
01:00:25.69	+38:47:17.5	−504.2	13.56	−0.66	−1.42	23.58	21.87
01:00:31.57	+38:44:49.2	−393.2	8.67	−0.96	−1.101	22.98	21.18
01:00:33.31	+38:47:36.2	−239.1	41.9	−1.16	−0.6722	23.24	21.94
01:00:42.01	+38:44:57.3	−229.1	7.31	−1	−0.1138	23.15	20.96
01:00:43.36	+38:46:32.3	−497.4	15.02	–	−1.931	24.45	21.18
01:00:45.42	+38:47:38.4	−302.4	15.83	−0.66	−1.144	23.59	21.88
01:00:46.31	+38:46:36.4	−382.4	16.62	−0.63	−0.7123	23.62	21.65
01:00:47.34	+38:46:13.4	−493	31.84	−1.08	−2.085	23.3	21.98
01:00:47.67	+38:46:53.0	−341.4	13.17	−0.77	−0.8154	23.39	21.5
01:00:53.79	+38:47:58.1	−166.8	8.33	–	−2.543	20.18	19.61
01:00:54.98	+38:44:22.9	−419.9	38.68	−0.92	−1.229	23.45	22.05
01:00:56.02	+38:45:19.6	−253.4	25.28	–	−1.675	21.32	20.57
01:00:58.50	+38:46:59.7	−317.4	10.78	–	−2.282	20.9	20.08
01:01:01.43	+38:46:30.6	−319.6	17.02	−1.22	−1.312	22.87	21.47
01:01:04.01	+38:48:43.0	−341.3	24.47	–	−2.343	21.33	20.37
01:01:15.28	+38:47:02.7	−175.8	3.57	–	−2.081	20.32	18.28

Table 6. Properties of candidate M31 halo stars in stream B region (field M6).

α (J2000)	δ (J2000)	v_r (km s^{-1})	v_{err} (km s^{-1})	[Fe/H]$_{phot}$	[Fe/H]$_{spec}$	v mag	I mag
01:08:31.0	37:30:21.6	−335.4	10.1	−0.91	−1.28	22.51	20.78
01:08:33.9	37:32:47.0	−292.3	6.571	−10.26	−2.74	22.49	21.6
01:08:34.8	37:29:19.1	−435.1	10.48	−0.2	–	23.94	21.94
01:08:36.4	37:34:00.4	−354.8	10.82	−0.03	−2.25	24.38	22
01:09:36.4	37:52:43.4	−317.3	7.16	−1.04	−0.97	22.74	21.25
01:09:36.4	37:52:57.4	−327.3	5.347	−0.67	–	23.08	21.37
01:08:36.5	37:25:16.6	−219.9	14.38	−0.36	−2.96	23.62	21.23
01:09:42.4	37:47:47.7	−369.9	13.09	−2.1	−1.61	22.26	20.99
01:09:43.1	37:41:33.4	−152.8	9.844	−0.58	−2.1	23.15	21.15
01:09:48.0	37:51:28.1	−307.8	11.37	−0.47	−0.18	23.61	20.89
01:09:50.9	37:43:20.3	−274.1	5.322	−1.17	–	23.39	22.1
01:09:53.9	37:52:18.1	−385.5	13.3	−0.64	−1.52	23.06	21.24

Table 7. Properties of candidate M31 halo stars in stream A region (field M8).

α (J2000)	δ (J2000)	v_r (km s^{-1})	v_{err} (km s^{-1})	[Fe/H]$_{phot}$	[Fe/H]$_{spec}$	v mag	I mag
01:18:11.4	36:12:51.4	−308.6	10.49	−1.58	−2.0	22.41	21.08
01:18:30.2	36:22:24.7	−178.1	9.126	−1.5	–	22.71	21.4
01:18:31.2	36:17:09.8	−178.4	6.106	−1.12	−1.88	22.38	20.83
01:18:32.0	36:13:03.5	−153.2	5.416	−1.41	−1.55	22.16	20.7

stars likely to be foreground MW contaminants (in the adopted velocity range of the M31 halo: < -150 km s^{-1}) by a factor of $\sim 3\times$ on average. In Fig. 2, the stars likely belonging to Stream 'C', and EC4 are highlighted (where EC4 member stars were preferentially inserted in the spectroscopic masks) allowing metallicity comparison to the fiducial globular cluster RGBs. To differentiate EC4 stars from the halo field, the velocities are also plotted against their radius from the EC4 centre. Fig. 2 shows that once the cluster, EC4, stars are removed, a strong metal-rich peak of stars at ~ -350 km s^{-1} dominates the stars kinematically identified to exclude the MW. The stars in this kinematic structure have average photometrically derived metallicity, [Fe/H] $= -0.74 \pm 0.19$. As the metallicity of

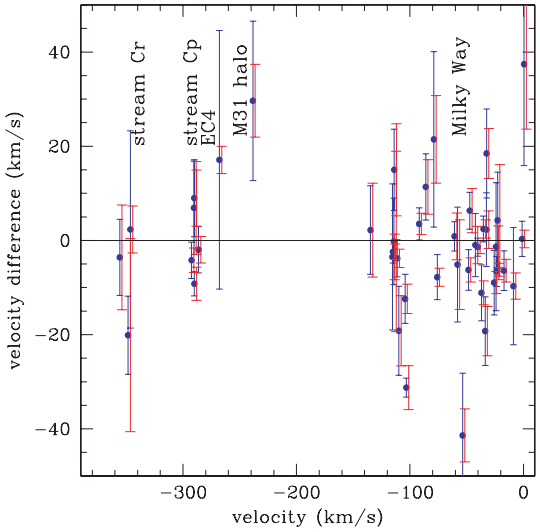

Figure 8. Velocity differences of stars lying in both fields F25 and F26. Stars identified to velocity regions likely associated to Stream 'Cr', Stream 'Cp', EC4, background M31 halo and MW foreground are identified. Stars are shown at their velocities from mask F25, with offset errorbars from mask F26.

this kinematic substructure is very similar to that measured for the total Stream 'C' ([Fe/H] = −0.6) by Ibata et al. (2007), this is an excellent candidate for a kinematic detection of Stream 'C'. Taking the clump of metal-rich stars $\pm 2\sigma$ from the peak, we find nine stars with an average $[v_r] = -349.5^{+1.8}_{-1.8}$, $\sigma_{v_r} = 5.1^{+2.5}_{-2.5}$km s^{-1}, where the individual velocity errors are taken into account in a maximum-likelihood sense. This procedure is described exactly in Martin et al. (2007), although no iterative clipping is done in this case as the contamination levels from foreground MW stars is much smaller. Briefly, using only the candidate Stream 'Cr' stars, a maximum-likelihood algorithm that explores a coarse grid of the (v_r, σ) space and searches for the couple of parameters that maximizes the *ML* function[1] defined as

$$ML(v_r, \sigma) = \sum_{i=1}^{N} \log \left\{ \frac{1}{\sigma_{tot}} \exp \left[-\frac{1}{2} \left(\frac{v_r - v_{r,i}}{\sigma_{tot}} \right)^2 \right] \right\} \quad (1)$$

with N the number of stars in the sample, $v_{r,i}$ is the radial velocity measured for the i^{th} star, $v_{err,i}$ is the corresponding uncertainty and $\sigma_{tot} = \sqrt{\sigma^2 + v^2_{err,i}}$. Using this definition of σ allows to disentangle the intrinsic velocity dispersion and the contribution of the measurement uncertainties to these likelihood distributions.[2] These distribution functions are shown in Fig. 9.

The velocity is close to the systemic velocity of M31, −300 km s^{-1}, which might be expected if the stream was truly close to tangential as it appears to be in the imaging (most of its velocity being orthogonal to our measured heliocentric component). We cannot estimate a reliable mass for the progenitor from this single spectroscopic measurement, as the stars we have detected lie off-centre from the Stream 'C' peak, and as yet we have not measured the full extent of the stream. None the less, we can at least place a constraint on the mass from the measured velocity dispersion in this field (Section 4).

By taking the average halo profile of Ibata et al. (2007) at this projected radius, ∼9 true halo stars are expected in fields F25/F26 (all stream structures removed from consideration), assuming all possible candidate RGBs have been observed in the two overlapping DEIMOS pointings, which they have. We find 26 halo stars are detected in the velocity region $v_{hel} < -150$ km s^{-1} excluding the MW, and after removing the high confidence EC4 stars (lying within two core radii) from consideration as they were added selectively to the mask in addition to the randomly selected halo stars. If nine stars are associated to Stream 'Cr' and as we will see another seven stars are associated to Stream 'Cp', there are 10 candidate halo stars found in the sample, in good agreement with the average prediction. Integrating the windowed $\sigma_v \sim 125$ km s^{-1} Gaussian of the halo, we find 3 per cent chance that a star lies in one of the three 10 km s^{-1} velocity bins encompassing this kinematic structure. At least one, but unlikely more than two of the candidate Stream 'Cr' stars will be unrelated halo. Therefore neither the metallicity nor velocity dispersion is likely to be heavily biased by unrelated halo stars. We note that ≪1 per cent Galactic contamination is expected at ∼ −350 km s^{-1}, from our own characterization of the MW population in our spectroscopic fields, from the Gilbert et al. (2006) analysis of MW dwarfs in their M31 spectroscopy, and from the Besançon Galactic populations model (as described in Ibata et al. 2005, 2007 and Chapman et al. 2006).

3.3 Stream 'Cp'

In analysing the velocity distribution of halo stars in field F25/26, we move on from the strong kinematic peak of stars at −349 km s^{-1} which we have identified with Stream 'Cr', and note in Fig. 2 a kinematic association of stars at $v_{hel} \sim -286$ km s^{-1} showing a remarkably small dispersion. Fig. 2 also plots the radial distance of the stars in the field from the cluster EC4, where it is apparent that this spike merges with likely EC4 member stars (Collins et al., in preparation). There are five stars lying within one core radius of EC4 (<30 pc), two borderline members between two and three core radii, and six candidate stream stars at such large distance that they are unlikely to be directly associated to EC4.

We note that one of these stars is likely either a blue supergiant star at M31 distance or is a MW contaminant, although the equivalent width of the Na I doublet is remarkably small for a MW dwarf (e.g. Guhathakurta et al. 2006; Martin et al. 2007), with the caveat that this example is very blue in colour where it is not clear Na I is a good discriminant (e.g. Koch et al. 2008). Since no photometric metallicity can be derived for this star, we will not consider it further in our analysis (the star is Stream 'Cp', 00:58:24.32+38:04:29.9).

A tight range in [Fe/H] = −1.26 ± 0.16 is observed in the five unambiguous Stream 'Cp' stars, very close to what we derive from the Ibata et al. (2007) foreground-subtracted photometry data set for the offset Stream 'Cp' region, [Fe/H] = −1.1. We propose that in addition to Stream 'Cr', we have also kinematically detected this lower contrast Stream 'Cp' in our fields F25/F26. It is a matter of debate how the two borderline EC4 stars are treated; starting from the Stream 'Cp' standpoint, we find no valid reason to reject them from the stream sample, as they lie well within the velocity window defined by the stars at much larger radius (see Fig. 2), although we quote our results with and without them. Again, the systemic velocity close to

[1] There is an error in this expression from Martin et al. (2007) which is corrected here.

[2] An alternative way to determine v_r and σ is to use $\sigma = \sigma'_{tot}$ in equation (1) to measure the observed dispersion and then correct from the mean velocity uncertainty, $\overline{v_{err}}$, such as $\sigma'_{tot} = \sqrt{\sigma^2 + \overline{v_{err,i}}^2}$. Parameters obtained in this way are similar to those given in the text.

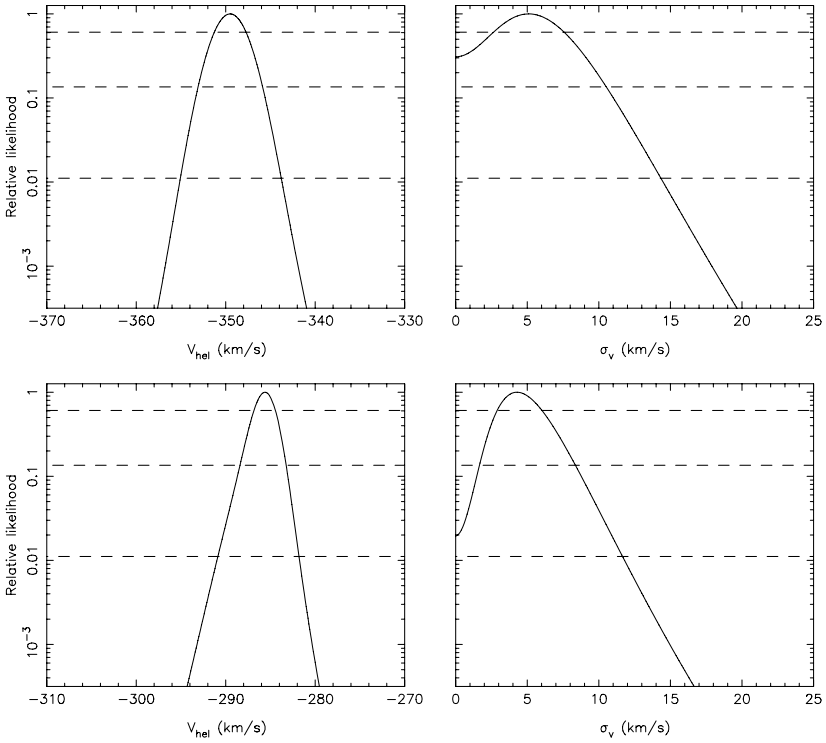

Figure 9. The kinematics of Stream 'C'. Upper panels: the relative-likelihood distribution (taking into account the measurement errors) of $\langle v_r \rangle$ and σ_{v_r} for velocities of Stream 'Cr' stars when marginalizing with respect to the other parameter. The thin dashed lines correspond, from top to bottom panel, to the parameter range that contains 68.3, 95.4 and 99.73 per cent of the probability distribution (1, 2 and 3 × σ uncertainties), revealing that Stream 'Cr' has a none-zero velocity dispersion at the 1σ level, and a remarkably small σ_{v_r}. The peak values and 1σ range are $\langle v_r \rangle = -349.5^{+1.8}_{-1.8}$ and σ_{v_r}=$5.1^{+2.5}_{-2.5}$. Lower panels: the same for Stream 'Cp' (with seven candidate members), showing a none-zero velocity dispersion at the >3 σ level. The peak values and 1σ range are $\langle v_r \rangle = -285.6^{+1.2}_{-1.2}$ and σ_{v_r}=$4.3^{+1.7}_{-1.4}$. Note that both streams have maximum-likelihood distributions close to symmetric about the solution in projection.

that of M31 ($v_{hel} = -285.6 \pm 1.2$ km s^{-1} with seven members, $v_{hel} = -285.0^{+1.7}_{-1.8}$ km s^{-1} with five members) would be consistent with the expected properties of a tangential stream. Using the maximum-likelihood technique, we calculate a true velocity dispersion of $\sigma_{v,corr} = 4.3^{+1.7}_{-1.4}$ km s^{-1} with seven members ($\sigma_{v,corr} = 5.1^{+2.5}_{-2.5}$ km s^{-1} with five members). The likelihood distribution functions are shown in Fig. 9.

The stacked spectra of Stream 'Cr' and Stream 'Cp' are shown in Fig. 10, emphasizing the clear difference in spectroscopically derived [Fe/H] (−0.9 versus −1.2) between the two kinematic peaks, in good agreement with the photometric [Fe/H] quoted in Table 1 (despite the fact that individual spectra are low S/N and show a large spread in [Fe/H]). With confidence that we have truly detected two different, superposed stream components through their offset kinematics and metallicities, we revisit the Stream 'C' region from Ibata et al. (2007). In Fig. 11, we show a zoomed-in region around Stream 'C', divided in [Fe/H] into two non-overlapping ranges (0.0 to −0.7, and −0.7 to −1.7). This division makes it clear that two physically separate structures are present, and we can attempt to separate the luminosities of the two components (see Section 4).

With conservatively only five member stars (the sixth not obviously being an RGB star), and a metallicity range well within that expected for M31's overall stellar halo ([Fe/H $\sim -1.4 \pm 0.2$ from Chapman et al. 2006; Fe/H ~ -1.2 along the minor axis in Kalirai et al. 2006 or Fe/H ~ -1.5 over the same minor axis fields in Koch et al. 2008), we should first consider how likely this kinematic peak is to be distinct from the smooth halo component. It is also of interest to demonstrate that these stars are not likely to be far-flung members of EC4.

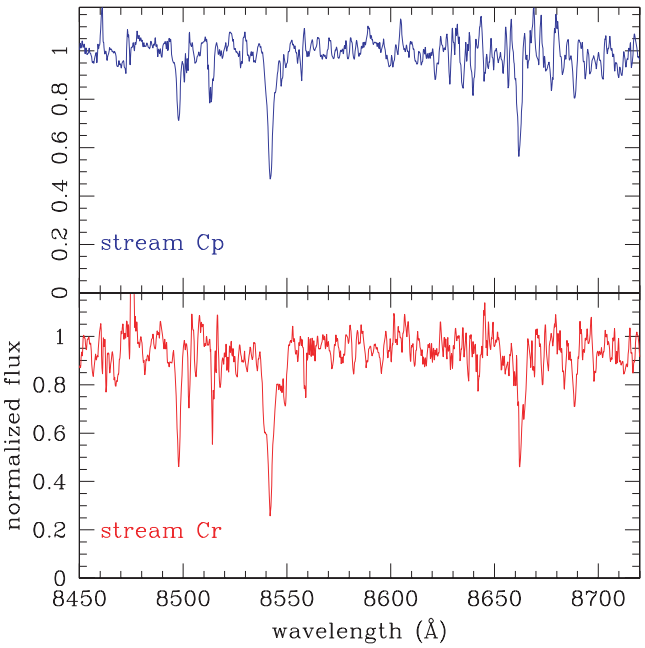

Figure 10. The stacked spectra of Stream 'Cr' and Stream 'Cp', weighting by the inverse variance in the continua, emphasizing the clear spectroscopic difference in [Fe/H] (−0.8 versus −1.2) between the two kinematic peaks, in good agreement with the photometric [Fe/H].

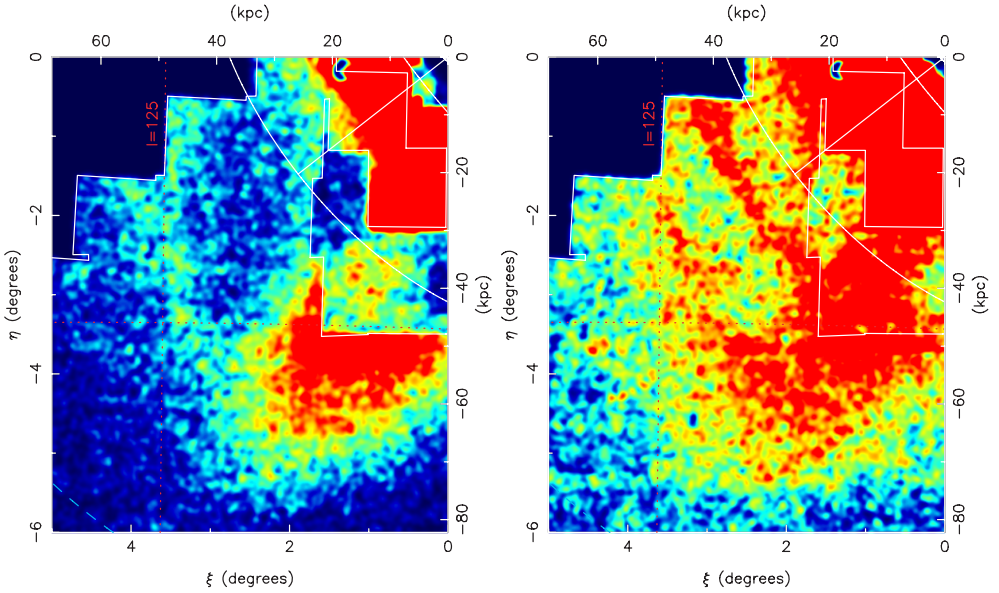

Figure 11. The Stream 'C' region shown zoomed-in (from fig. 20 of Ibata et al. 2007, which details the definitions of cutout regions etc.) with slices in [Fe/H] ($-0.7 <$ [Fe/H] < 0.0 – left-hand panel; $-1.7 <$ [Fe/H] < -0.7 – right-hand panel) allowing the spatially offset Stream 'Cr' (left-hand panel) and Stream 'Cp' (right-hand panel) components to clearly be seen. Our kinematic separation of these two components appears to be reflected in physically distinct (but somewhat overlapping) regions. The comparison also highlights the much more metal-poor Stream 'D' in the right-hand panel.

These five stars at large radii from EC4 (0.7 to 10.3 arcmin, or 150 to 2220 pc), chosen by chance in the spectroscopic masks are unlikely to be bound members of EC4 itself. First, these stars would represent 5–74 core radii of EC4 (30 pc). It is implausible that stars this far from the centre belong to the cluster unless it is strongly disrupted, or is in fact only the cold core component of a more diffuse dwarf galaxy with an outer second component of stars. EC4 does not show any obvious signs of disruption, but given the faintness of EC4, it is difficult to tell from the HST/ACS image in Mackey et al. (2006) whether there are subtle signatures of disruption. It can also be seen in Fig. 2 that the metallicities of these stars appear to be marginally richer than EC4, although photometric errors from EC4 star crowding could easily account for these differences.

It is more difficult to differentiate these stars from M31 halo stars than it is for Stream 'Cr' stars, since the peak of the halo velocity distribution lies at ~ -300 km s^{-1}, although the very broad velocity dispersion $\sim$125 km s^{-1} at this projected radius (Chapman et al. 2006) makes it less likely to find such a strong spike of stars at -286 km s^{-1}. We estimate the chance association specifically as follows. We assume we know nothing about EC4 and that we have an ensemble of stars which are the members of the M31 halo. For this purpose, we assume conservatively that a halo star is any star consistent with the halo CMD, and to coarsely remove Galactic contaminants, lying within $-550\,\mathrm{km\,s^{-1}} < v_\mathrm{r} < -150\,\mathrm{km\,s^{-1}}$, or roughly $\pm 2\sigma$ with a window clip appropriate to the Galactic contaminant distribution in Fig. 2. Removing the stars specifically targeted to lie in EC4, there are 26 stars which satisfy these criteria. There is a 3.2 per cent chance that any given halo star will lie in the 10 km s^{-1} window centred on the five unambiguous Stream 'Cp' stars systemic velocity (-285 km s^{-1}). This is a conservative assessment since the chance would be much lower for a window offset from the ~ -300 km s^{-1} peak of the M31 halo distribution. However, the chance that five stars out of 26 lie in this window is extremely small (irrespective of how the window is defined, the probability is consistently below $<10^4$), given the broad halo σ_v. This estimate is even more conservative as there is in fact a substantial contribution from the Stream 'Cr' stars in this halo field – a better estimate of the total underlying halo stars would be $\sim$16. We can conclude that these five stars represent a rare kinematic spike in a smooth halo distribution.

3.4 The continuations of Stream 'C'

As described in Section 2, upon detecting cold kinematic peaks plausibly attributed to Stream 'C', we observed an additional Keck/DEIMOS field (F36) further north along this structure. The properties of this field are shown in Fig. 3. While no prominent peaks are found in the velocity distribution of this northern field, a concentration of five metal-rich ([Fe/H] ~ -0.7) stars is observed at an average velocity of -350 km s^{-1}, possibly attributable to the same Stream 'Cr' structure, and thereby showing no obvious velocity gradient.

In the same field (F36), we also search for the more metal-poor Stream 'Cp'. We find a clump of four similarly metal-poor stars, $\langle$[Fe/H]$\rangle = -1.2$, at an average velocity of -246 km s^{-1}, offset by $\sim +40$ km s^{-1} from the Stream 'Cp' and EC4 peak in fields F25/26.

Orbit models of these streams will be presented in a future paper, while Fardal et al. (2008) discuss how these stream-like structures could conceivably be related to the Giant Southern Stream.

3.5 The extended star cluster, EC4

Fig. 2 shows that stars targeted in the cluster, EC4, have clearly been kinematically identified with a distribution of velocities centred at $v_\mathrm{hel} = -282.1^{+3.3}_{-3.4}$ km s^{-1} (see Collins et al., in preparation, for details). The EC4 stars have [Fe/H]$_\mathrm{phot} = -1.4 \pm 0.1$.[3] After

[3] Mackey et al. (2006) find [Fe/H]$_\mathrm{phot} = -1.84$ for EC4 from *HST* photometry and simultaneous fitting of the RGB and Horizontal Branch. This difference is explored carefully in Collins et al. (in preparation).

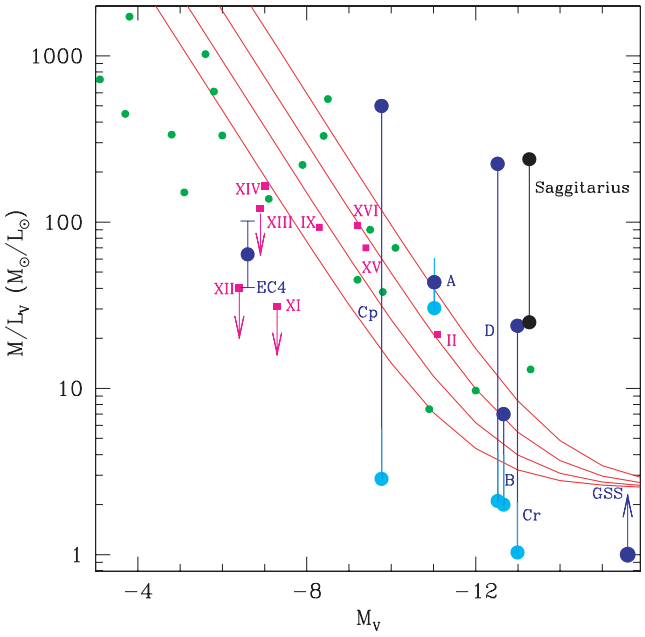

Figure 12. Comparison of the M/L and light, M_v for the streams in M31, the Sgr stream in the MW (Majewski et al. 2003), and compared to the faint dwarf galaxies from both the MW (Simon & Geha 2007; Martin et al. 2007) and M31 with central velocity dispersion estimates. The procedure for measuring the M/L is described in the text. Stream M/L values are shown as bars connecting the structural mass estimate to the σ_v estimate. A factor of 2 uncertainty is shown for the σ_v mass since we are likely observing the streams at especially cold points between turning, and the true progenitor mass is likely two to four times larger. And XI, And XII and And XIII (Collins et al., in preparation) are all shown as upper limits, since their velocity dispersions are all unresolved by their measurements – the 1σ-likelihood contour is used to set a tentative limit. EC4 measurements come from Collins et al. (in preparation), while AndXV, AndXVI measurements come from Letarte et al. (2008). The solid lines are curves of constant dark matter halo mass ($1, 2, 4, 8 \times 10^7$ M$_\odot$ from bottom to top panel), assuming a stellar mass-to-light ratio of 2.5 M$_\odot$/L$_\odot$.

carefully considering the night-to-night velocity systematics, Collins et al. (in preparation) conclude that EC4 has a none-zero velocity dispersion at the $>2\sigma$ level. As these stars were preselected to lie in EC4, we assume that at least the five stars lying within one core radii of the EC4 centre (and possibly the two stars at two to three core radii) can be removed from the surrounding M31 halo sample for our statistical analysis of the Stream 'C' in previous sections. We have clearly identified the systemic velocity of EC4 as being compatible with the Stream 'Cp' kinematics.

3.6 Stream 'D'

Based on the example of Stream 'Cr' and Stream 'Cp', we are motivated to search for a narrow velocity peak in the case of Stream 'D'. However, Fig. 4 showing the CMD, radial velocities and metallicities (as for the previous streams) does not reveal any obvious detection of stars in this stream. We proceed by comparing the expected metallicity from Ibata et al. (2007), $-1.7 < [\mathrm{Fe/H}] < -0.7$, with any stars in the 'halo' sample [culled from the velocity and EW(Na I) cuts] which could be the Stream 'D'. We highlight all stars in the CMD which could conservatively be consistent with the Stream 'D' median [Fe/H] $= -1.2$. There are no obvious kinematic spikes within these colour-selected stars, as shown in Fig. 4 (right-hand panel). However, there is an isolated group of two stars within a 10 km s^{-1} bin at -405 km s^{-1}. Two stars at ~ -400 km s^{-1} are somewhat unexpected (8 per cent chance) given the halo velocity dispersion at a projected radius of 35 kpc (Chapman et al. 2006). There are no better candidates for the Stream 'D' than this pair of RGB stars, but we cannot confidently separate Stream 'D' stars from spheroidal halo stars.

In the DEIMOS field placed further along Stream 'D' (field F37), an kinematic association of five stars stands out again at $\sim$400 km s^{-1} (as with field F7 above), however only three have inferred [Fe/H] within a range consistent with the photometric properties. If these stars represent the Stream 'D', there is also no measurable velocity gradient detected, as found for Stream 'Cr'. In Table 1, we present the velocity dispersion measured from the five plausible Stream 'D' stars combined from both fields ($\sigma_{v_\mathrm{r}} =$ 4.2 km s^{-1}). However, the low contrast of Stream 'D' relative to the background M31 halo, together with our inability to distinguish with confidence a kinematic identification means that these results are tentative. Much larger numbers of spectroscopic measurements along Stream 'D' are required in order to reliably detect a coherent structure in velocity.

3.7 Streams 'A' and 'B'

The other two streams lying perpendicular to the minor axis presented in Ibata et al. (2007), Stream 'A' and Stream 'B' lie at 120 and 80 kpc, respectively. Both of these streams have serendipitous spectroscopic pointings lying in their edge regions from Gilbert et al. (2006) and Koch et al. (2008), named fields M8 and M6, respectively, in their nomenclature (see Ibata et al. 2007 for placements of these spectroscopic pointings in the wider M31 halo map). We present the CMDs, velocity histograms and metallicities for Stream 'B' and Stream 'A' here for analysis (Figs 6 and 7).

In field M8 (Stream 'A'), there are only four stars with velocity measurements attributable to the M31 halo. The clump of three stars at -172 km s^{-1} have an [Fe/H] $= -1.3$ on average, very similar to the statistical measurement of the [Fe/H] ~ -1.3 in Stream 'A' (Ibata et al. 2007). We further suggest, along Ibata et al. (2007) and Koch et al. (2008), that these three kinematically identified *halo* stars are more likely to be associated to the stellar halo of M33 (the Triangulum galaxy), given the M31 halo velocity dispersion (Chapman et al. 2006) shown in Figs 6 and 7. It is therefore worth considering that this Stream 'A' structure might actually be disrupted remains of a satellite in M33's halo. The dispersion of these three stars, 14.5 km s^{-1}, cannot easily be deconvolved for measurement errors using the maximum-likelihood approach. Instead, since the errors are similar for all three stars, we write as in footnote (1) $\sigma_{v,\mathrm{corr}} = \sqrt{(\sigma_v^2 - \sigma_{\mathrm{instr}}^2)} = \sqrt{(14.5^2 - 7.2^2)} = 12.5$ km s^{-1}.

We carry out the same procedure as with the other streams, identifying candidate stars in the CMD which are consistent with the average metallicity found in Ibata et al. (2007) for the streams in question. In field M6 (Stream 'B'), a kinematic peak of stars lying at ~ -330 km s^{-1} with $\langle$[Fe/H]$\rangle \sim -1.0$ represents a reasonable candidate for this stream. Notably, this metallicity is very close to that estimated for Stream 'B' in Ibata et al. (2007), and further, both the metallicity and the velocity distribution in this field depart significantly from the average found in Koch et al. (2008) for the outer halo. Again following the logic of our discussions in the streams 'C' and 'D', the RGB overdensity in this field attributed to the stream should statistically result in the bulk of stars kinematically detected lying in the stream structure. Removing these five relatively metal-rich stars from the halo sample leaves six more metal-poor stars

which would represent the surrounding M31 halo at this radius. As with the Stream 'A' case above, we simply estimate an intrinsic dispersion directly from these five candidate Stream 'B' stars, using their average measurement error, of σ_{v_r}=6.9 km s^{-1}.

4 THE STREAMS IN THE CONTEXT OF THE DWARF SPHEROIDAL M/L TO L RELATION

It is of interest to ask how the properties of these streams would compare to other M31 satellites if treated as dwarf remnants. As described in Ibata et al. (2007), the light in polygonal regions surrounding each stream was integrated, with background corrections applied. Here, we go further to emphasize the metal-poor region of Stream 'C' defined as the v-band light with $-2.0 <$ [Fe/H] < -1.0, and further assuming (through the luminosity ratios of the offset portions of the metal-poor and metal-rich components, described above) that 1/10 of this metal-poor light belongs to Stream 'Cp' while the other 9/10 belongs to Stream 'Cr'. The resulting luminosities are summarized in Table 1. There is, of course, an uncertainty in the M_v estimates, since the streams are terminated by the edge of our M31 halo imaging to the North. We will therefore simply assume here that the M_v estimates are lower limits.

The width of the streams can provide constraints on the mass of the progenitor, since debris from more massive satellites is likely to produce wider debris streams that spread more rapidly along the orbit with time. We measure the widths of all our streams by taking the minor axis profile integrated over the full extent where the streams are detected. The streams are not always exactly orthogonal to the minor axis, however they are close enough (and in any case not always well defined) that any broadening introduced by this simple procedure should be minimal. We then fit Gaussians to the profile, subtracting the local background from regions on either side of each stream. We quote the full width at half-maximum (FWHM) in Table 1.

Johnston, Sackett & Bullock (2001) present simple analytic scalings for the width and length of debris streams, with the main assumption that the progenitor is supported by random motions. In this case, the measured fraction, $s \equiv w/R$, of the width to the radial distance to the stream is related to the mass m of the satellite through the relation

$$s = [Gm/(v_{\rm circ}^2 R_{\rm peri})]^{1/3}.$$

Font et al. (2006) estimate the progenitor mass of the Giant Southern Stream (GSS) in M31 using these measurements (w, R) and an orbit model suggesting $R_{\rm peri} = 3$–4.5 kpc, finding 1.0–1.6 $\times$ 10^8 M$_\odot$. With an updated luminosity for the GSS from the wider survey of Ibata et al. (2007), 1.5 $\times$ 10^8 M$_\odot$, the M/L $\sim$1 M$_\odot$/L$_\odot$. We note, however, that if the models of the GSS progenitor as rotationally supported (Fardal et al. 2008; Mori & Rich 2008) are correct, this would invalidate the Font et al. estimate of progenitor mass.

We do not yet have sufficient information to model the orbits of these five fainter streams in M31, and thus our estimates of the progenitor masses are slightly less secure than the GSS estimate in Font et al. (2006), with a linear dependence on the uncertain $R_{\rm peri}$. We place limits on $R_{\rm peri}$ by assuming that we are seeing these streams at apocentre, and that orbits in cosmological simulations have average $R_{\rm peri}/R_{\rm apo} \sim 0.2$– 0.25 (Ghigna et al. 1998; van den Bosch et al. 1999; Benson 2005). These limits are listed in Table 1 along with the other model parameters (and taking for M31, $v_{\rm circ}$ = 260 km s^{-1}).

The same procedure can also be applied to the Sgr stream, taking parameters from Majewski et al. (2003), with $R_{\rm peri} = 12$, $w_{\rm FWHM} = 4$ and $v_{\rm circ} = 220$ kpc, we calculate a mass of 5.5 $\times$ 10^9 M$_\odot$. Majewski et al. (2003) derive a mass from kinematics of Sgr of 5.8 $\times$ 10^8 M$_\odot$ with a M/L = 25 ($M_v = -13.27$).

The velocity dispersions of the streams can also be used to constrain the progenitor masses, although perhaps with even less accuracy. Generally, the dispersion in stream debris should decrease over time (Helmi & White 1999). If these streams were very young, we would not expect dynamical cooling to be significant yet. Tidal interactions with dark matter substructure in the halo may also not have had sufficient time to significantly heat the streams if they are relatively young (Ibata et al. 2002; Johnston, Spergel & Haydn 2002). Helmi & White (1999) suggest the velocity dispersion should vary most significantly in an oscillatory manner as a function of radial orbital phase.

Font et al. (2006) also estimate the progenitor mass of the GSS from a single σ_{v_r}=15 km s^{-1} lying between apocentre and pericentre along the stream, with a lower limit of 10^8 M$_\odot$, consistent with their estimate from structural/orbit properties. As predicted by Helmi & White (1999), the stream can become very cold in between the turning points with the velocity dispersion of the stream reaching values well below the central dispersion of the satellite, and as small as $\sigma/\sigma_0 \sim 0.5$.

In a similar manner, we can estimate the M/L of the streams presented in this contribution. For all the streams, we can apply the methodology of Font et al. (2006) directly as we have plausible kinematic detections in each case, along with reasonable constraints on the stream widths and morphologies. We expect the velocity dispersion of the progenitor to be as large or larger than the intrinsic value estimated for the stream and assume mass follows light (Richstone & Tremaine 1986). For Stream 'D', we have taken the combined σ_{v_r} from both spectroscopic pointings (Table 1), assuming that the ~ -400 km s^{-1} stars are the most likely members of the structure. For Stream 'A', we assume the three halo stars at -172 km s^{-1} represent the stream (although as discussed, it is ambiguous whether it is a structure associated to M31 or M33). The results of our mass estimates are presented in Table 1, and plotted on Fig. 12, where we highlight a factor of 2 uncertainty given that we are likely observing the streams at especially cold points between turning.

However, we caution that these M/L ratios have significant uncertainties attached. The progenitor may not be completely disrupted, the velocity dispersion could be a very poor mass estimate (more typically a lower limit) depending on where in the orbit and evolution the stream is, and from the truncation of the image to the north, we already know the observed luminosity may not be representative for the entire streams.

The comparison of the streams with the MW satellites and all published M31 satellites is presented in Fig. 12. Stream M/L values are shown as bars connecting the structural mass estimate to the σ_v estimate. The Mateo (1998) relation between M/L and the luminosity of a dwarf galaxies in the Local Group has also been plotted on Fig. 12. The relation can be understood physically as more massive dwarfs retaining more of their gas (and therefore arriving at $z = 0$ with a lower M/L ratio), while lower mass haloes more easily expel their gas and form smaller numbers of stars. All of our newly constrained M31 streams are in agreement with the relation within reasonable errors, which is somewhat surprising given our limited ability to constrain the masses of the streams. Interestingly, the Sgr stream lies significantly above the relation over all plausible mass estimates. Many of the new M31 dSphs, along with most MW dSphs fall on the relation, although And X, And XII, as clearly

appear to be outliers (as discussed in Collins et al., in preparation), as are many of the new faint MW dSphs (Simon & Geha 2007). This suggests that at the low-mass end, a range of processes beyond simply the feedback in winds which explains galaxies as massive as our stream progenitors may truncate star formation (e.g. Ricotti & Gnedin 2005), or else the numerous model assumptions are failing when reaching these faint limits. It will be of interest to obtain improved constraints on these M31 streams and model their orbits, to see if progenitor mass estimates continue to keep them on the Mateo relation.

5 DISCUSSION

Our spectroscopic survey of the M31 faint streams has yielded an encouraging initial census of the kinematics, however it is clear from our results that significant efforts with a 10-m telescope are required to usefully constrain the kinematic properties of the streams for modelling. At least in the case of the spatially overlapping Stream 'Cr' and Stream 'Cp', it is remarkable that we have been able to clearly distinguish these structures by kinematics. Indeed, it was not entirely clear from initial inspection of the imaging in Ibata et al. (2007) that there were two different streams in this vicinity at all. Only careful inspection of the imaging divided in slices of metallicity reveals two structures slightly offset spatially.

The cluster, EC4, lies in a region where the metal-poor Stream 'Cp' has roughly 50 per cent the stellar density of the metal-rich Stream 'Cr', although our spectroscopy reveals that EC4 is likely related to Stream 'Cp' with Stream 'Cr' overlapping only in projection. Could Stream 'Cp' actually be the debris from disrupted EC4 material? The integrated luminosity of Stream 'Cp' within the MegaCam survey is comparable to a small dwarf galaxy like And XV or And XVI (Letarte et al. 2008), $M_v \sim -9.5$, which would suggest the baryonic matter mass-loss of EC4 ($M_v = -6.6$, Mackey et al. 2006) would be dramatically larger than its current *intact* mass. No distortion of the EC4 isophotes is found in the *HST* imaging of Mackey et al. (2006) (Tanvir et al., in preparation), although the faintness of EC4 means this is unlikely to be a good test of ongoing mass-loss or tidal distortion. We have, however, noted that the outer stars in EC4 show a statistically significant velocity shift from the inner EC4 stars, similar to the Stream 'Cp' stars in the field surrounding EC4. This could happen for instance if EC4 were disrupting in a stream along the line of sight. Regardless, it is likely that Stream 'Cp' and EC4 are at least related by their kinematics and metallicities, EC4 possibly representing an intact system carried along in the disrupted progenitor represented by Stream 'Cp'. If EC4 is dark matter dominated, we have in fact detected the very first *sub-subhalo* (i.e. a galaxy that was bound to a satellite galaxy), possibly explaining its small ($r_c = 30$ pc) size. From a Λcold dark matter cosmological point of view, the LMC and Small Magellanic Cloud should also have such sub-subhaloes with $L \sim 10^7$–$10^8\,L_\odot$, but we find none (and here we cannot invoke tidal disruption of these systems, because they seem to be falling in for the first time). Of course, it also remains the possibility that EC4 has nothing to do with the Stream 'C' structure at all. Without precise distance information, it is difficult to rule this out completely.

We also ask whether these stream structures could be related to the giant southern stream imaged in Ibata et al. (2001, 2007)? As we have noted, the metallicities of various streams all differ, only Stream 'Cr' and Stream 'B' being even close to the metallicity of the core region of the giant southern stream (Ibata et al. 2001, 2004; Guhathakurta et al. 2006; Ibata et al. 2007). However, in the CFHT-MegaCam survey, the outer region of the GSS is more metal-poor and has a metallicity that is similar to that of some of the more metal-poor streams. None the less, the general impression from the low dispersion of the streams in kinematics, their physical thickness and varying (but narrow) metallicities makes it hard to reconcile with a scenario whereby these stream structures as an ensemble are related to the giant southern stream.

Fardal (2008, and private communication) has modelled the stream resulting from a GSS progenitor that is flattened and rotating like a disc, building on the constraints and models from Fardal et al. (2007) and Gilbert et al. (2007). Because it is on such a radial orbit, when it reaches pericentre very close to M31, part of the progenitor could be on the opposite side of M31 to the rest, depending on the orientation of the disc. This means that it starts orbiting M31 in the opposite direction to the rest and leaves debris in different physical locations than the main stream. The disc-like kinematics results in caustic structures that appear similar to streams or arcs. In this model, the new streams from Ibata et al. (2007), and herein, would be shells from this counter-orbiting part of the stream. Assuming a large metallicity gradient in the progenitor, they would have a much lower metallicity than the main stream since they come from an outer part of the progenitor.

Whether or not this specific model is correct, the general idea that the progenitor was physically quite large, and passed extremely near the centre of M31, means that debris could get thrown out in all directions. Given the metallicity structure of the progenitor, it is plausible that some of this debris could have distinct metallicities but be ultimately related to the same progenitor. While somewhat implausible for the reasons stated above, it remains to be seen if the specific kinematics and metallicities of our new observations can be reproduced in such a model.

Whereas the photometric profiles could only remove Galactic contamination and stars belonging to stream substructures statistically, we can explicitly remove stars belonging to the streams (and the MW) by their kinematics and assess the underlying M31 stellar halo density from 30 to 120 kpc on the minor axis. While our resulting measurement has so few stars as to be highly uncertain statistically, it does reveal the general power of kinematic analysis of the M31 halo population.

It is remarkable the extent to which these kinematic substructures projected on the minor axis dominate the halo star statistics in these fields. In the fields studied, they represent approximately two-third of the candidate halo stars, revealing that the photometric minor axis profile from Irwin et al. (2005) and Ibata et al. (2007) is significantly flattened by such structures. We are led to the likely conclusion that stellar haloes are made up of multiple kinematically cold streams, perhaps even to the extent proposed by Bullock & Johnston (2005) (see also Bell et al. 2008).

6 CONCLUSIONS

In conclusion, we have conducted a Keck/DEIMOS spectroscopic survey of five stellar streams, recently uncovered through deep imaging observations of the halo.

(i) We have uncovered a kinematic substructure at $v_{\rm hel} = -349.5 \pm 1.8$ km s^{-1} from a spectroscopic field lying in the Ibata et al. (2007) Stream 'C'. The cold component has $\sigma_{v_{\rm r}}$=5.1±2.5 and a narrow range in [Fe/H] $= -0.7 \pm 0.2$, which we propose represents a metal-rich component, Stream 'Cr'.

(ii) We have uncovered a second kinematic substructure in the same field as Stream 'Cr' at $v_{\rm hel} = -285.6 \pm 1.2$ km s^{-1} with $\sigma_{v_{\rm r}} = 4.3^{+1.7}_{-1.4}$ km s^{-1} (non-zero at $>3\sigma$ confidence interval) and a

narrow range in [Fe/H] $= -1.3 \pm 0.2$, which we propose represents a metal-poor stream, Stream 'Cp'. We demonstrated that this kinematic Stream 'Cp' has a counterpart in a spatially offset metal-poor region of Stream 'C' in Ibata et al. (2007).

(iii) We plausibly detect both Stream 'Cr' and Stream 'Cp' at a position $\sim$30 kpc further north along the structure, with no detectable velocity gradient for Stream 'Cr', and a measured velocity gradient of $\sim$40 km s^{-1} for Stream 'Cp'.

(iv) We were unable to identify kinematic substructure unambiguously associated to Stream 'D' from our serendipitous spectroscopic pointing, however subsequent spectroscopy well centred in the Stream 'D' identifies a likely cold kinematic structure which has a viable counterpart in the serendipitous pointing. We propose a kinematic detection of Stream 'D' at $v_{\rm hel} = -390.5$ km s^{-1} with $\sigma_{v_{\rm r}} = 4.2$ km s^{-1}.

(v) Spectroscopy near the edges of Stream 'A' and Stream 'B' suggests a likely kinematic detection for Stream 'B' with $v_{\rm hel} \sim -330$, $\sigma_{v,{\rm corr}} \sim 6.9$ km s^{-1}, and a kinematic detection of Stream 'A' at $v_{\rm hel} \sim -172$, $\sigma_{v_{\rm r}} \sim 12.5$ kms^{-1}. Neither spectroscopic pointing in these streams is ideally placed, and additional spectroscopic observations are well motivated to further constrain the kinematics of these structures.

(vi) The extended cluster EC4 lies in the Stream 'C' region, with kinematics ($v_{\rm hel} = -282$), and metallicity ([Fe/H] $= -1.4$) which suggest it is related to the more metal-poor stream Stream 'Cp'. EC4 could be the progenitor of the metal-poor Stream 'Cp' (somewhat unlikely given the apparent stellar mass difference between the stream and EC4), or it may simply be a structure carried along by the disrupted stream progenitor. In this case, and if EC4 is dark matter dominated, we have in fact detected the very first *sub-subhalo* (i.e. a galaxy that was bound to a satellite galaxy), possibly explaining its small ($r_{\rm c} = 30$ pc) size.

(vii) By explicitly removing stars belonging to the streams by their kinematics, we can assess the underlying M31 stellar halo density and metallicity on the minor axis. This contrasts the purely photometric approach where Galactic contamination and stars belonging to stream substructures can only be removed statistically. Our resulting halo measurement has so few stars as to be highly uncertain statistically, however, it does reveal the general power of kinematic analysis of the halo population for future endeavors. The fraction of background halo stars in these stream fields suggests the conclusion that stellar haloes are largely made up of multiple kinematically cold streams.

ACKNOWLEDGMENTS

We thank an anonymous referee for a very careful reading and a helpful report. We thank Mark Fardal for helpful discussions on the giant southern stream. SCC acknowledges NSERC and the Canadian Space Agency for support. RMR and AK acknowledge support from AST-0309731.

REFERENCES

Bell E. et al., 2008, ApJ, 680, 295
Belokurov V. et al., 2006, ApJ, 642, 137L
Belokurov V. et al., 2007, ApJ, 658, 337
Benson A., 2005, MNRAS, 358, 551
Brodie J., Larsen S., 2002, AJ, 124, 1410
Bullock J., Johnston K., 2005, ApJ, 635, 931
Chapman S., Ibata R., Ferguson A. M. N., Lewis G., Irwin M., Tanvir N., 2005, ApJ, 632, L87
Chapman S., Ibata R., Lewis G., Ferguson A. M. N., Irwin M., McConnachie A., Tanvir N., 2006, ApJ, 653, 255
Chapman S. C. et al., 2007, ApJ, 662, 79
Davis M. et al., 2003, Proc. SPIE, 4834, 161
Faber S. et al., 2003, Proc. SPIE, 4841, 1657
Fardal M., Guhathakurta P., Babul A., McConnachie A. W., 2007, MNRAS, 380, 15
Fardal M., Babul A., Guhathakurta P., Gilbert K., Dodge C., 2008, ApJ, 682, L33
Fellhauer M. et al., 2006, ApJ, 651, 167
Font A., Johnston K., Guhathakurta P., Majewski S., Rich M., 2006, AJ, 131, 1436
Gilbert K. et al., 2006, ApJ, 652, 1188
Gilbert K. et al., 2007, ApJ, 668, 245
Girardi L., Grebel E., Odenkirchen M., Chiosi C., 2004, A&A, 422, 205
Ghigna S., Moore B., Governato F., Lake G., Quinn T., Stadel J., 1998, MNRAS, 300, 146
Guhathakurta P. et al., 2006, AJ, 131, 2497
Helmi A., White S. D. M., 1999, MNRAS, 307, 495
Helmi A., White S. D. M., de Zeeuw P. T., Zhao H. S., 1999, Nat, 402, 53
Huxor A., Tanvir N., Irwin M., Ibata R., Collett J., Ferguson A., Bridges T., Lewis G., 2005, MNRAS, 360, 1007
Huxor A., Tanvir N., Ferguson A., Irwin M., Ibata R., Bridges T., Lewis G., 2008, MNRAS, 385, 1989
Ibata R., Irwin M., Lewis G., Ferguson A. M. N., Tanvir N., 2001, Nat, 412, 49
Ibata R., Lewis G., Irwin M., Quinn T., 2002, MNRAS, 332, 915
Ibata R., Chapman S., Ferguson A., Irwin M., Lewis G., 2004, MNRAS, 351, 117
Ibata R., Chapman S., Fergusson A., Lewis G., Irwin M. J., Tanvir N., 2005, ApJ, 634, 287
Ibata R., Chapman S., Irwin M., Lewis G., Martin N., 2006, MNRAS, 373, 70
Ibata R., Martin N. F., Irwin M., Chapman S., Ferguson A. M. N., Lewis G. F., McConnachie A. W., 2007, ApJ, 671, 1591
Irwin M. J., Ferguson A., Ibata R., Lewis G., Tanvir N., 2005, ApJ, 628, L105
Johnston K. V., Sackett P. D., Bullock J. S., 2001, ApJ, 557, 137
Johnston K. V., Spergel D. N., Haydn C., 2002, ApJ, 570, 656
Kalirai J. et al., 2006, ApJ, 648, 389
Koch A. et al. 2008, ApJ, submitted (arXiv:0711.4588)
Larsen S. S., Brodie J. P., 2000, AJ, 120, 2938
Majewski S., Skrutskie M., Weinberg M. D., Ostheimer J. C., 2003, ApJ, 599, 1082
Martin N. F., Ibata R. A., Irwin M. J., Chapman S. C., Lewis G. F., Ferguson A. M. N., Tanvir N., McConnachie A. W., 2006, MNRAS, 371, 1983
Martin N., Ibata P., Chapman S., Irwin M., Lewis G., 2007, MNRAS, 380, 281
Martinez-Delgado D., Penarrubia J., Gabany R., Trujillo I., Majewski S., Pohlen M., 2008, ApJ, preprint (arXiv:0805.1137)
Mateo M., 1998, ARA&A, 36, 435
Mackey D. et al., 2006, ApJ, 653, 105
McConnachie A., Irwin M., Ferguson A., Ibata R., Lewis G., Tanvir N., 2005, MNRAS, 356, 979
Mori M., Rich M., 2008, ApJ, 674, L77
Peng E. et al., 2006, ApJ, 639, 838
Peñarrubia J., McConnachie A., Babul A., 2007, ApJ, 650, 33
Peñarrubia J., McConnachie A., Navarro J., 2008a, ApJ, 672, 904
Peñarrubia J., Navarro J., McConnachie A., 2008b, ApJ, 673, 226
Richstone D., Tremaine S., 1986, AJ, 92, 72
Ricotti M., Gnedin N., 2005, ApJ, 629, 259
Schiavon R. P., Barbuy B., Rossi S., Milone A., 1997, ApJ, 479, 902
Simon J., Geha M., 2007, ApJ, 670, 313
van den Bosch F. C., Lewis G. F., Lake G., Stadel J., 1999, ApJ, 515, 50

This paper has been typeset from a TEX/LATEX file prepared by the author.